

1  
2  
3 **Live-imaging of endothelial Erk activity reveals dynamic and sequential**  
4 **signalling events during regenerative angiogenesis**  
5

6 Kazuhide S. Okuda<sup>1,2,3,4</sup>, Mikaela S. Keyser<sup>4</sup>, David B. Gurevich<sup>5,6</sup>, Caterina  
7 Sturtzel<sup>7,8</sup>, Elizabeth A. Mason<sup>1,2,3</sup>, Scott Patterson<sup>1,2,3,4</sup>, Huijun Chen<sup>4</sup>, Mark Scott<sup>4</sup>,  
8 Nicholas D. Condon<sup>4</sup>, Paul Martin<sup>5</sup>, Martin Distel<sup>7,8</sup>, Benjamin M. Hogan<sup>1,2,3,4#</sup>  
9

10  
11 <sup>1</sup>*Organogenesis and Cancer Program, Peter MacCallum Cancer Centre, Melbourne, VIC 3000,*  
12 *Australia*

13 <sup>2</sup>*Sir Peter MacCallum Department of Oncology, University of Melbourne, Melbourne, VIC 3000,*  
14 *Australia*

15 <sup>3</sup>*Department of Anatomy and Physiology, University of Melbourne, Melbourne, VIC 3000, Australia*

16 <sup>4</sup>*Institute for Molecular Bioscience, The University of Queensland, St Lucia, QLD 4072, Australia*

17 <sup>5</sup>*School of Biochemistry, Biomedical Sciences Building, University Walk, University of Bristol, Bristol*  
18 *BS8 1TD, United Kingdom*

19 <sup>6</sup>*Department of Biology and Biochemistry, University of Bath, Claverton Down, Bath, BA2 7AY, United*  
20 *Kingdom*

21 <sup>7</sup>*Innovative Cancer Models, St Anna Kinderkrebsforschung, Children's Cancer Research Institute,*  
22 *1090 Vienna, Austria*

23 <sup>8</sup>*Zebrafish Platform Austria for preclinical drug screening (ZANDR), 1090 Vienna, Austria*  
24  
25  
26  
27  
28  
29  
30  
31  
32

33 *Author for Correspondence:*

34 # Professor Ben Hogan  
35 Organogenesis and Cancer Program,  
36 Peter MacCallum Cancer Centre,  
37 Melbourne, VIC 3000, Australia  
38 E-mail: [ben.hogan@petermac.org](mailto:ben.hogan@petermac.org)  
39

40  
41 **Keywords:** Erk, Vegfr, Angiogenesis, Endothelial cell, Regeneration, Zebrafish.  
42

43 **Abstract**

44

45 The formation of new blood vessel networks occurs via angiogenesis during  
46 development, tissue repair and disease. Angiogenesis is regulated by intracellular  
47 endothelial signalling pathways, induced downstream of Vascular endothelial growth  
48 factors (VEGFs) and their receptors (VEGFRs). A major challenge in understanding  
49 angiogenesis is interpreting how signalling events occur dynamically within  
50 endothelial cell populations during sprouting, proliferation and migration. Erk is a  
51 central downstream effector of Vegf-signalling and reports the signalling that drives  
52 angiogenesis. We generated a vascular Erk biosensor transgenic line in zebrafish  
53 using a kinase translocation reporter that allows live-imaging of Erk-signalling  
54 dynamics. We demonstrate the utility of this line to live-image Erk activity during  
55 physiologically relevant angiogenic events. Further, we reveal dynamic and  
56 sequential endothelial cell Erk-signalling events following blood vessel wounding.  
57 Initial signalling is dependent upon  $Ca^{2+}$  in the earliest responding endothelial cells,  
58 but is independent of Vegfr-signalling and local inflammation. The sustained  
59 regenerative response however, involves a Vegfr-dependent mechanism that  
60 initiates concomitant with the wound inflammatory response. This work reveals a  
61 highly dynamic sequence of signalling events in regenerative angiogenesis and  
62 validates a new resource for the study of vascular Erk-signalling in real-time.

63

64

65



## 66 **Introduction**

67 The formation of new blood vessels from pre-existing vasculature (angiogenesis) is a  
68 fundamental process central in the formation of a viable embryo and in the  
69 pathogenesis of many diseases (Carmeliet and Jain, 2011; Chung and Ferrara,  
70 2011; Potente et al., 2011). Angiogenesis is controlled by intricately regulated cell-  
71 cell, cell-matrix and intracellular signalling events. The activity of extracellular signal-  
72 regulated kinase (ERK) downstream of the vascular endothelial growth factor A  
73 (VEGFA)/VEGF receptor 2 (VEGFR2) signalling pathway is essential for both  
74 developmental and pathological angiogenesis (Koch and Claesson-Welsh,  
75 2012; Simons et al., 2016). ERK-signalling is also required downstream of  
76 VEGFC/VEGFR3 signalling in lymphangiogenesis (Deng et al., 2013). ERK is  
77 required for angiogenic sprouting, proliferation and migration, with genetic or  
78 pharmacological inhibition of ERK-signalling resulting in impaired blood vessel  
79 development in zebrafish and mice (Srinivasan et al., 2009; Costa et al.,  
80 2016; Nagasawa-Masuda and Terai, 2016; Shin et al., 2016a). Cancer-associated  
81 vessels have high ERK activity and inhibition of ERK-signalling blocks cancer-  
82 associated angiogenesis in mice (Wilhelm et al., 2004; Murphy et al., 2006). Beyond  
83 the formation of new vessels, ERK-signalling is also essential to maintain vascular  
84 integrity in quiescent endothelial cells (ECs) (Ricard et al., 2019), altogether  
85 demonstrating a central role for ERK in vascular biology.

86

87 Despite its importance, vascular ERK-signalling has largely been examined with  
88 biochemical assays or in tissues in static snapshots. Numerous studies have  
89 suggested that ERK-signalling is likely to be highly dynamic during angiogenic  
90 events, for example studies that examine Erk activation using antibodies to detect  
91 phosphorylated Erk (pErk) have observed changes associated with increased EC  
92 signalling, EC motility and specific EC behaviours (Costa et al., 2016; Nagasawa-  
93 Masuda and Terai, 2016; Shin et al., 2016a). In zebrafish, live-imaging of blood ECs  
94 at single cell-resolution coupled with carefully staged immunofluorescence staining  
95 for pErk suggested that an underlying dynamic Erk-signalling event may control tip-  
96 cell maintenance in angiogenesis (Costa et al., 2016). Nevertheless, EC signalling  
97 dynamics at the level of key intracellular kinases, such as ERK, remain poorly  
98 understood. This gap in our understanding is largely due to a gap in our ability to  
99 live-image changes in signalling as they occur.

100

101 A number of new biosensors have now been applied *in vitro* and *in vivo* that allow  
102 live-imaging of proxy readouts for intracellular signalling events (reviewed in detail in  
103 (Shu, 2020)). One approach used, has involved application of biosensors that utilise  
104 fluorescence resonance energy transfer (FRET)-based readouts. The first ERK  
105 FRET-based biosensor (ERK activity reporter (EKAR)) was developed in 2008  
106 (Harvey et al., 2008). Since then, modifications had been made to improve sensitivity  
107 and dynamic range and to generate other ERK FRET-based biosensors such as  
108 EKAR-EV, RAB-EKARev, and sREACH (Komatsu et al., 2011;Ding et al., 2015;Tang  
109 and Yasuda, 2017;Mehta et al., 2018). Importantly, these ERK FRET-based  
110 biosensors had been applied *in vivo* to visualise ERK-signalling dynamics in various  
111 cell types during development, cell migration, and wound healing (Kamioka et al.,  
112 2012;Mizuno et al., 2014;Goto et al., 2015;Hiratsuka et al., 2015;Kamioka et al.,  
113 2017;Takeda and Kiyokawa, 2017;Sano et al., 2018;Wong et al., 2018). While ERK  
114 FRET-based biosensors have been widely reported, they are limited in requiring  
115 extensive FRET controls and a low speed of acquisition for FRET based imaging.  
116 More recently, Regot and colleagues generated the ERK-kinase translocation  
117 reporter (KTR)-Clover construct (hereafter referred to as EKC), that allows for  
118 dynamic analysis of ERK activity using a readout not involving FRET. A  
119 fluorescence-based kinase activity reporter translates ERK phosphorylation events  
120 into a nucleo-cytoplasmic shuttling event of a synthetic reporter (Regot et al., 2014).  
121 Thus, the KTR system allows rapid quantifiable measurements of ERK activity based  
122 upon subcellular localisation of a fluorescent fusion protein, and is more sensitive to  
123 phosphatase-mediated kinase activity downregulation when compared to other  
124 commonly used reporters. This has been applied to enable dynamic ERK-signalling  
125 pulses to be analysed at single-cell resolution both *in vitro* and also *in vivo* (Regot et  
126 al., 2014;de la Cova et al., 2017;Mayr et al., 2018;Goglia et al., 2020;Pokrass et al.,  
127 2020;De Simone et al., 2021), where it has demonstrated to be of high utility.

128

129 In this study, we generated a vascular EC-restricted EKC zebrafish transgenic strain  
130 and assessed its utility to study angiogenesis *in vivo*. We apply real-time  
131 quantification of Erk-signalling dynamics during developmental angiogenesis and  
132 vessel regeneration. We validate methods to quantify Erk activity during real time  
133 imaging that will be applicable in a variety of settings in vascular biology and beyond.

134 Demonstrating the promise of this approach, we here identify an immediate early  
135 Erk-signalling response to wounding of vasculature that is Ca<sup>2+</sup> signalling dependent  
136 and distinct from a later Vegfr-driven regenerative response. Overall, this work  
137 reports a unique resource for imaging of vascular signalling and further illuminates  
138 mechanisms of vascular regeneration following wounding.

139

140

## 141 **Results**

### 142 **Generation of a zebrafish EC-EKC transgenic line**

143 KTRs utilise a kinase docking and target site that is juxtaposed to a phospho-  
144 inhibited nuclear localization signal (NLS) and attached to a fluorescent tag (Regot et  
145 al., 2014). Upon kinase activity the NLS is inactive and the fluorescent tag detected  
146 in the cytoplasm; when the kinase is not active, dephosphorylated NLS leads to  
147 increased nuclear localisation. The EKC module that we took advantage of here  
148 relies upon the well characterised ERK-dependent transcription factor ELK1, utilising  
149 the ERK docking site (**Figure 1A**) (Chang et al., 2002;Regot et al., 2014) This  
150 reporter has previously been shown to report Erk activity *in vivo* (de la Cova et al.,  
151 2017;Mayr et al., 2018;Pokrass et al., 2020;De Simone et al., 2021). To visualise  
152 real-time Erk-signalling in ECs, we expressed this reporter under the control of an  
153 EC-specific promoter (*fli1aep* (Villefranc et al., 2007)) (**Figure 1A-E**). Blood vessel  
154 development was unaffected in *Tg(fli1aep:EKC)* transgenic embryos and larvae  
155 (**Figure 1B-E**). Furthermore, transgenic adults displayed no adverse morphological  
156 features and were fertile (data not shown), indicating that EKC does not inhibit Erk-  
157 signalling *in vivo*, or cause developmental phenotypes and consistent with previous  
158 findings (Mayr et al., 2018;De Simone et al., 2021).

159

160 To test if the *Tg(fli1aep:EKC)* line reports vascular Erk-signalling, embryos were  
161 treated with either DMSO, mitogen-activated protein kinase kinase (MEK) inhibitor  
162 SL327, or pan-VEGFR inhibitor SU5416, and vascular EKC localisation examined at  
163 27 hpf. Tip ECs in developing ISVs have been shown to have high Erk activity  
164 (Costa et al., 2016;Nagasawa-Masuda and Terai, 2016;Shin et al., 2016a) and we  
165 observed nuclear depleted EKC localisation in leading angiogenic ISV cells including  
166 at the level of the dorsal longitudinal anastomosing vessel (DLAV) in DMSO treated  
167 embryos. (**Figure 1F-F'',I**). In contrast, ISV ECs of embryos treated with either

168 SL327 or SU5416 had nuclear enriched EKC localisation indicating inactive Erk-  
169 signalling (**Figure 1G-I**). To best visualise these differences in signalling and  
170 differences shown below, we used a heat map of nuclear EC EKC intensity that is  
171 inverted so that blue-scale indicated low signalling (nuclear enriched) and red-scale  
172 indicates high signalling (nuclear depleted) (**Figure 1F''-H''**). Therefore, we  
173 confirmed that the *Tg(fli1aep:EKC)* (hereafter EC-EKC) transgenic line enables  
174 quantification of Erk activity in developing ECs.

175

176

### 177 **The EC-EKC line enables visualisation and quantification of dynamic Erk** 178 **activity during primary angiogenesis**

179 We next sought to determine whether the EC-EKC line reports physiologically  
180 relevant Erk-signalling events. Using immunofluorescence staining, ISV tip cells that  
181 sprout from the dorsal aorta (DA) have been shown to have higher Erk-signalling  
182 than ECs that remain in the DA during the initiation of angiogenesis (Nagasawa-  
183 Masuda and Terai, 2016;Shin et al., 2016a). We examined 22 hpf embryos and  
184 indeed observed that sprouting ISV ECs display high Erk activity based upon EKC  
185 localisation (**Figure 1-figure supplement 1A-B**). However, many DA ECs also  
186 appeared to have nuclear depleted EKC localisation (**Figure 1-figure supplement**  
187 **1A**, yellow arrows). To compare EKC and Erk-signalling levels between sprouting  
188 tip-cells and the DA, we utilised multiple methods. We found that measuring the  
189 nuclear/cytoplasm EKC intensity ratio in DA ECs was inaccurate because DA ECs  
190 are irregular in morphology, making cytoplasmic quantification unreliable (**Figure 1-**  
191 **figure supplement 1A'**). Previous studies have compared nuclear EKC with nuclear  
192 H2B-mCherry intensity in the same cell as a ratio to measure Erk activity (e.g. in  
193 vulval precursor cells in the worm (de la Cova et al., 2017)). We assessed the ratio  
194 of nuclear EKC/H2B-mCherry intensity in double transgenic EC-  
195 EKC;*Tg(fli1a:H2B:mCherry)* embryos and found that the ISV tip cells had higher Erk  
196 activity than adjacent DA “stalk” ECs (**Figure 1-figure supplement 1A'' and C**). We  
197 used a stable *Tg(fli1a:H2B-mCherry)* transgenic line with consistent H2B-mCherry  
198 intensity. Next, we investigated whether nuclear EKC intensity alone was sufficient to  
199 compare Erk-signalling between ECs. The ratio of nuclear EKC intensity of the  
200 sprouting ISV tip-cell and the adjacent DA “stalk” EC clearly showed higher signalling  
201 in tip-cells and was consistent with EKC/H2B-mCherry measurements (**Figure 1-**

202 **figure supplement 1C**). Thus, we establish that both methods can be reliably used,  
203 when measurement of nuclear/cytoplasm EKC intensity is not possible because of  
204 difficulty identifying a cells cytoplasm. We compare nuclear EKC intensities for  
205 analyses hereafter.

206

207 Next, we correlated EC Erk-signalling state (based on EKC intensity) with a cells  
208 migratory state (based on nuclear ellipticity) as previous studies have suggested a  
209 correlation (Costa et al., 2016). At 28 hpf, ISV tip cells were either located above the  
210 horizontal myoseptum with elliptical nuclei indicative of a migrating EC, or at the level  
211 of the future DLAV, with less-elliptical (oblate) nuclei indicative of a non-migrating EC  
212 (**Figure 1-supplement 1D-F**). We found that migrating ECs had higher Erk activity  
213 than non-migrating ECs, irrespective of their tip or stalk cell location in an ISV  
214 (**Figure 1-figure supplement 1D-G**). This is consistent with previous studies of  
215 Vegfa/Kdr/Kdrl/Erk signalling in zebrafish ISVs (Yokota et al., 2015;Costa et al.,  
216 2016;Nagasawa-Masuda and Terai, 2016;Shin et al., 2016a) and confirms a strong  
217 correlation between ISV EC motility and EC Erk-signalling.

218

219 Using carefully staged immunofluorescence analyses, it was previously suggested  
220 that when tip cells divide in ISV angiogenesis, daughter cells show asymmetric  
221 Kdrl/Erk signalling that re-establishes the tip/stalk EC hierarchy (Costa et al., 2016).  
222 However, an analysis of fixed material can only ever imply underlying dynamics. To  
223 investigate the dynamics of Erk-signalling upon tip-cell division, we performed high-  
224 speed time-lapse imaging of ISV tip ECs as they undergo mitosis in 24 hpf embryos.  
225 Immediately preceding cell-division, ECs display cytoplasmic localisation of H2B-  
226 mCherry due to the disruption of the nuclear membrane (**Figure 2A**, yellow arrow).  
227 High-speed live-imaging of ISV tip ECs revealed nuclear enriched EKC localisation  
228 during cell division (**Figure 2A-C**), which was maintained until cytokinesis (**Figure**  
229 **2B, Video 1**) but may reflect nuclear membrane breakdown rather than altered  
230 cellular signalling. Subsequently, daughter ECs in the tip position progressively  
231 increased their Erk activity, while ECs in the trailing stalk daughter position remained  
232 nuclear enriched, showing asymmetric Erk-signalling activity rapidly following cell  
233 division (**Figure 2B-I, Video 1**). To accurately assess this across multiple  
234 independent tip-cell divisions, we measured the ratio of tip/stalk daughter cell nuclear  
235 EKC intensity over time. This revealed that tip cells consistently increased their Erk

236 activity relative to stalk cells in a progressive manner with the most dramatic  
237 asymmetry observed ~21 minutes post-cytokinesis (**Figure 2J,K, Video 1**).  
238 Collectively, the EC-EKC line enabled quantitative assessment of physiologically  
239 relevant Erk activity by real-time live imaging and confirmed previously suggested  
240 asymmetric signalling post tip-cell division.

241

### 242 **Vessel wounding induces rapid Erk activation**

243 As a major downstream target for VEGFA/VEGFR2 signalling, ERK is essential for  
244 stimulating ectopic sprouting of otherwise quiescent mature vessels (Wilhelm et al.,  
245 2004;Murphy et al., 2006). However, Erk-signalling dynamics during pathological  
246 angiogenesis have not been analysed in detail. To determine whether the EC-EKC  
247 line can be used to dynamically visualise Erk activation in ECs in pathological  
248 settings, we analysed EC Erk activity following vessel wounding using a laser  
249 ablation method. We chose this model because vessel wounding in 4 dpf larvae  
250 results in highly reproducible Vegfa/Kdr/Kdrl signalling-dependent vessel  
251 regeneration (Gurevich et al., 2018). Importantly, cell wounding induces ERK-  
252 signalling *in vitro* and *in vivo* in other settings (Matsubayashi et al., 2004;Li et al.,  
253 2013;Hiratsuka et al., 2015;Aoki et al., 2017;Mayr et al., 2018).

254

255 To visualise Erk-signalling dynamics following cellular ablation and vessel wounding,  
256 we time-lapse imaged both ablated ISV ECs and the adjacent non-ablated ISV ECs  
257 in 4 dpf EC-EKC larvae for 20 minutes before and for 22 minutes after vessel  
258 wounding (**Figure 3A-C**). As a control, ISV ECs of unablated 4 dpf larvae were time-  
259 lapse imaged for the same period. EKC localisation in the majority of ISV ECs  
260 indicated low basal Erk-signalling in ECs of mature vessels (**Figure 3D,D',F,F',H,I,**  
261 **Videos 2-5**). Upon vessel wounding, Erk activity in ablated ISV ECs immediately  
262 increased (**Figure 3E,E',H,I, Videos 3 and 4**). Surprisingly, Erk activity in ECs of  
263 ISVs located adjacent to the ablated ISV (termed adjacent ISV) also rapidly  
264 increased (**Figure 3G,G',H,I, Videos 3 and 5**). Although the activation of Erk-  
265 signalling in adjacent ISV ECs was slower than in ablated ISV ECs, the level of Erk  
266 activation in ablated and adjacent vessels was comparable by 15 minutes post-  
267 ablation (mpa, green dotted line) and consistent up to 22 mpa (**Figure 3I**). Both  
268 venous and arterial ECs equally showed Erk activation 15 mpa in ablated ISVs post-

269 vessel wounding, suggesting that both venous and arterial ECs are able to rapidly  
270 activate Erk-signalling (**Figure 3J**). Finally, to understand the relationship between  
271 Erk activation in vessels and distance from the wound, we measured the response of  
272 ECs in immediately adjacent, 2<sup>nd</sup> adjacent and 3<sup>rd</sup> adjacent ISVs from the ablated  
273 ISV (in an anterior direction). We found that the activation of Erk signalling was  
274 largely limited to the wounded and immediately adjacent ISVs (**Figure 3-figure  
275 supplement 1**).

276

### 277 **The initial rapid Erk-signalling response is not induced by macrophages or** 278 **Vegfr activity**

279 Macrophages recruited to a wound site have been shown to provide a local source of  
280 Vegfa that stimulates vessel regeneration (Gurevich et al., 2018). Therefore, we  
281 investigated whether macrophages are required for rapid Erk activation in ISV ECs.  
282 As previously reported (Gurevich et al., 2018), macrophage recruitment to the wound  
283 was minimal at 15 mpa, while robust macrophage recruitment was observed 3 hours  
284 post-ablation (hpa), suggesting that macrophages may not contribute to rapid Erk  
285 activation (**Figure 3-figure supplement 2A-D**). We depleted macrophages by  
286 knocking down Spi-1 proto-oncogene b (Spi1b) and Colony stimulating factor 3  
287 receptor (Csf3r) using established morpholino oligomers (Rhodes et al., 2005;Ellett  
288 et al., 2011;Pase et al., 2012) (**Figure 3-figure supplement 2E-G**). We found that  
289 depletion of macrophages led to a quantifiable but mild reduction in normal vessel  
290 regeneration measured at 24 hpa in this model (**Figure 3-figure supplement 2H-J**).  
291 The rapid EC Erk activation post-wounding was unaffected upon macrophage  
292 depletion (**Figure 3K, Figure 3-figure supplement 2K-V'**). We next tested whether  
293 Vegfr-signalling was required for this rapid Erk activation. Erk activation in both  
294 ablated and adjacent ISV ECs 15 mpa was blocked in larvae treated with SL327,  
295 indicating that it requires upstream Mek activation (**Figure 3L, Figure 3-figure  
296 supplement 3D-M'**). However, treatment with two independent and validated  
297 VEGFR-inhibitors, SU5416 (**Figure 1H-I**) and AV951 (**Figure 3-figure supplement  
298 3A-C**), did not impair the rapid Erk activation at 15 mpa (**Figure 3L, Figure 3-figure  
299 supplement 3O-Z'**). Therefore at 15 mpa, Erk activation in both ablated and  
300 adjacent ISV ECs is induced independently of either macrophages or Vegfr-  
301 signalling, suggesting an initial response to vessel wounding that has not been  
302 previously examined.

303

304 **Following the initial rapid Erk activation, signalling is progressively restricted**  
305 **to regenerating vessels**

306 Previous studies have shown that local wounding induces a rapid burst in ERK-  
307 signalling in surrounding cells (Matsubayashi et al., 2004;Li et al., 2013;Hiratsuka et  
308 al., 2015;Aoki et al., 2017;Mayr et al., 2018). To determine whether the initial Erk  
309 activation in ISV ECs post-vessel wounding was maintained, Erk activity was  
310 followed over a longer time-course until 3 hpa, when robust macrophage recruitment  
311 was observed (**Figure 3-figure supplement 2C,D**). Erk activity was again increased  
312 upon vessel wounding in both ablated and adjacent ISV ECs at 15 mpa (**Figure 4A-**  
313 **D, Figure 4-figure supplement 1A-I'**). Erk activity was maintained until 30 mpa in  
314 adjacent ISV ECs, but then gradually decreased and returned to non-ablated control  
315 levels by 1 hpa (**Figure 4B-D**). By contrast, high Erk activity was maintained for the  
316 duration in ablated ISV ECs (**Figure 4A,A',C,D**). To test if this difference in Erk  
317 activity was influenced by long-term time-lapse imaging, Erk-signalling was analysed  
318 in ISV ECs of 3 hpa larvae. Similar to the time-course analysis, Erk activity in ablated  
319 ISV ECs was high at 3 hpa, while ECs in adjacent ISVs were at non-ablated control  
320 level (**Figure 4-figure supplement 1J-N**).

321

322 Given that the initial rapid burst of Erk activation progressively returns to basal levels  
323 in unwounded vessels, we assessed if this was a general wound response. We  
324 examined the initial Erk-signalling burst in muscle and skin cells following a large  
325 puncture wound using a ubiquitous EKC strain (Mayr et al., 2018). This confirmed  
326 that an initial activation of Erk signalling in cells surrounding the puncture wound was  
327 only transient (**Video 6**) and in this case was progressively lost even in cells at the  
328 immediate site of the wound, unlike in regenerating vessels. To further investigate  
329 whether only regenerating ISVs maintain high Erk activity after wounding, tissue in  
330 between the ISVs was ablated without injuring the ISVs in 4 dpf EC-EKC larvae  
331 (termed control ablation hereafter). Erk activity in surrounding ISV ECs was analysed  
332 at 15 mpa and 3 hpa. Similar to vessel ablation, this adjacent tissue ablation resulted  
333 in rapid activation of Erk-signalling in ISV ECs (**Figure 4-figure supplement 2A-C**).  
334 Erk activity in these ECs decreased to non-ablated control levels by 3 hpa (**Figure 4-**  
335 **figure supplement 2A-C**). Therefore, Erk-signalling is immediately activated in



336 muscle, skin epithelial and ECs upon injury, but only regenerating vessels retain this  
337 high activity at 3 hpa upon vessel wounding.

338

### 339 **Vegfr-signalling drives ongoing Erk activity to control vessel regeneration**

340 We next examined if ongoing Erk activity in ablated ISV ECs was maintained by  
341 Vegfr-signalling consistent with earlier reports (Gurevich et al., 2018). To test this,  
342 we analysed Erk activity of ablated ISV ECs in 3 hpa larvae treated with inhibitors of  
343 the Kdr/Kdrl/Mek/Erk signalling pathway. Treatment with SL327 inhibited Erk  
344 activation at 3 hpa, as did treatment with the Vegfr-inhibitor SU5416 (**Figure 5A,**  
345 **Figure 5-figure supplement 1A-F',I-J'**). Furthermore, we used an F0 CRISPR  
346 approach (Wu et al., 2018) to generate *kdrl* knockout embryos (termed *kdrl* crispant  
347 hereafter). These embryos phenocopied earlier reported mutant and morphant  
348 phenotypes (**Figure 5-figure supplement 1K,L**) (Habeck et al., 2002;Covassin et  
349 al., 2006). 3 hpa F0 crispant larvae displayed reduced Erk activity in EC-EKC  
350 measurements compared with ISV ablation control larvae (**Figure 5B, Figure 5-**  
351 **figure supplement 1M-T'**). Unlike drug treated larvae, *kdrl* crispants displayed a  
352 mild reduction in Erk activity, likely due to compensation from other Vegfrs, such as  
353 Kdr, and/or Flt4 (zebrafish orthologue of VEGFR3) (Covassin et al., 2006;Shin et al.,  
354 2016b). Overall, these genetic and pharmacological approaches indicate that  
355 Vegfr/Mek signalling is required for sustained high Erk activity in ablated ISV ECs at  
356 3 hpa. To determine the functional relevance of this in ongoing regeneration, we  
357 treated embryos following ablation-based wounding with SU5416 or two independent  
358 Mek inhibitors: SL327 and Trametinib. We observed that inhibition of Vegfr- or Erk-  
359 signalling completely blocked all ongoing vessel regeneration (**Figure 5C, Figure 5-**  
360 **figure supplement 1U-X**). Finally, we found no difference in EC-EKC activation at 3  
361 hpa in the absence of macrophages, suggesting that macrophages play a  
362 modulatory role in vessel regeneration and are not the sole source of Vegfs in this  
363 laser ablation model (**Figure 5D, Figure 5-figure supplement 2**).

364

365 Interestingly, we noted that while treatment with SU5416 at 10  $\mu$ M blocked ongoing  
366 Erk activation (**Figure 5A, Figure 5-figure supplement 1I-J'**), treatment with the  
367 same inhibitor at a lower dose of 4  $\mu$ M did not completely block Erk activity (**Figure**  
368 **5A, Figure 5-figure supplement 1G-H'**). To further investigate this with more spatial

369 resolution, we examined Erk activity in ISV ECs relative to their distance from the  
370 cellular ablation site. Erk-signalling in the first, second, and third ISV ECs from the  
371 wound was activated 3 hpa in control larvae, while treatment with 10  $\mu$ M SU5416  
372 inhibited signalling in ECs located in all of these positions (**Figure 5E,G,H, Figure 5-**  
373 **figure supplement 1C-D',I-J'**). However, with the intermediate dose of 4  $\mu$ M  
374 SU5416, while the closest cell to the wound site still displayed Erk activity, as did the  
375 second cell from the wound site, the third and furthest from the wounded sites were  
376 now inhibited (**Figure 5F,H, Figure 5-figure supplement 1G-H'**). These results  
377 suggest that there is a gradient of Vegfr/Erk signalling activity in the ablated ISV ECs  
378 resulting in higher Vegfr/Erk activity in ECs closer to the wounded site, which can  
379 only be inhibited with SU5416 at higher concentrations. To test this, we examined  
380 the EC EKC levels relative to cell position and directly confirmed this graded  
381 activation at 3 hpa (**Figure 5I, Figure 4-figure supplement 1J-M'**). Together, these  
382 analyses confirm that during the ongoing response to vessel wounding, Vegfr-  
383 signalling is crucial and drives a positionally graded signalling response to regulate  
384 regenerating vessels.

385

### 386 **Ca<sup>2+</sup> signalling is required for initial rapid Erk activation upon vessel wounding**

387 Although Vegfr-signalling is required for sustaining high Erk activity in ablated ISV  
388 ECs, it is not required for inducing the initial rapid Erk-signalling response. Activated  
389 by ATP released by damaged cells, Ca<sup>2+</sup> signalling is one of the first intra-cellular  
390 mechanisms to be activated post-wounding in many cell types (reviewed in detail in  
391 (Ghilardi et al., 2020)). Accordingly, mechanical injury of blood vessels has been  
392 shown *in situ* to rapidly activate Ca<sup>2+</sup> signalling in neighbouring endothelial cells in  
393 excised rat aorta (Berra-Romani et al., 2008;Berra-Romani et al., 2012). Although  
394 Ca<sup>2+</sup> signalling activates Erk-signalling in endothelial cells downstream of the  
395 Vegfa/Vegfr2 signalling pathway (Koch and Claesson-Welsh, 2012;Moccia et al.,  
396 2012), Ca<sup>2+</sup> signalling alone can also activate Erk-signalling (Xiao et al., 2011;Handly  
397 et al., 2015).

398

399 To determine whether Ca<sup>2+</sup> signalling is rapidly activated in ablated ISV ECs in our  
400 model, we measured the dynamic expression of a ubiquitously expressed GCamp, a  
401 GFP-based Ca<sup>2+</sup> probe, using the *Tg(actb2:GCaMP6f);Tg(kdrl:mCherry-CAAX)*

402 transgenic line (Herzog et al., 2019). We used a validated transgenic line which has  
403 previously demonstrated a general  $\text{Ca}^{2+}$  wound response and  $\text{Ca}^{2+}$  signalling in brain  
404 tumours and associated microglia (Chia et al., 2019;Herzog et al., 2019). We  
405 observed a general response in tissue surrounding the ablated site (data not shown),  
406 as well as active  $\text{Ca}^{2+}$  signalling in immune cells (**Figure 6A, Videos 7,8**, as  
407 previously described in (Yoo et al., 2012;Razzell et al., 2013;de Oliveira et al.,  
408 2014;Beerman et al., 2015;Herzog et al., 2019;Poplimont et al., 2020)) in the same  
409 movies analysed below, validating the utility of this line. ISVs in non-ablated 4 dpf  
410 larvae did not show  $\text{Ca}^{2+}$  signalling, indicating low  $\text{Ca}^{2+}$  activity in stable ISVs  
411 (**Figure 6B, Video 7**). In contrast, ablated ISV ECs showed a rapid pulse of active  
412  $\text{Ca}^{2+}$  signalling at 5mpa, which progressively decreased and returned to the level of  
413 the surrounding tissue (**Figure 6A,B, Video 8**). Active  $\text{Ca}^{2+}$  signalling was not  
414 observed in adjacent ISVs (**Figure 6A,B, Video 8**). To determine whether  $\text{Ca}^{2+}$   
415 signalling is required for rapid Erk activation in ablated ISV ECs, 4 dpf EC-EKC  
416 larvae were treated with either DMSO or a potent  $\text{Ca}^{2+}$  signalling inhibitor Nifedipine  
417 for 30 minutes. Nifedipine treatment did not inhibit Erk-signalling activation in  
418 adjacent ISV ECs resulting in similar Erk activity as DMSO treated larvae 15 mpa  
419 (**Figure 6C, Figure 6-figure supplement 1A-B',G-J'**). However, Erk activation in  
420 ablated ISV ECs (where we observed the GCaMP signal above) was significantly  
421 reduced when compared to DMSO treated larvae (**Figure 6C, Figure 6-figure**  
422 **supplement 1C-F'**). This was reproduced in an independent experiment using  
423 Amlodipine, an alternative  $\text{Ca}^{2+}$  signalling inhibitor (**Figure 6D, Figure 6-figure**  
424 **supplement 1K-T'**). This indicates that  $\text{Ca}^{2+}$  signalling plays a crucial role upstream  
425 of Erk in the wound response, but also that the response is differentially regulated in  
426 ablated compared with adjacent vessels, indicative of additional underlying signalling  
427 complexity.

428

429 We next tested whether  $\text{Ca}^{2+}$  signalling is required for maintaining Erk activity in  
430 ablated ISV ECs 3 hpa. To assess ongoing signalling, 4 dpf EC-EKC larvae were  
431 treated with either DMSO or Nifedipine 30 minutes prior to the 3 hpa timepoint.  
432 Activation of Erk-signalling in ablated ISV ECs 3 hpa was not inhibited by Nifedipine  
433 (**Figure 6E, Figure 6-figure supplement 2A-G'**). Inhibition of  $\text{Ca}^{2+}$  signalling  
434 immediately following wounding between 0 and 30 mpa also had no impact on later  
435 Erk signalling at 3 hpa (**Figure 6F, Figure 6-figure supplement 2H-N'**). Thus,  $\text{Ca}^{2+}$

436 signalling is required for rapid Erk activation, but not for maintaining Erk activity in  
437 ablated ISV ECs. In the analysis of  $\text{Ca}^{2+}$  signalling following vessel wounding, we  
438 noted that this transient pulse of  $\text{Ca}^{2+}$  signalling was highest in the ECs closest to the  
439 wounded site (**Video 8**). Thus, we further sought to determine if Erk-signalling in ECs  
440 closest to the wound activates first during the initial dynamic induction. Quantitative  
441 analysis based on multiple movies (including **Video 3**), showed that Erk-signalling in  
442 ECs proximal to the wounded site (first and second positioned ECs) activated first,  
443 followed by ECs further away from the wounded site (third, fourth and fifth ECs)  
444 (**Figure 6G**). Quantitatively the ECs proximal to the ablation site (first and second  
445 positioned ECs) showed the highest magnitude of difference from control, and this  
446 difference reduced as ECs were positioned further from the ablation site (**Figure**  
447 **6H**). This shows that like the initial burst in  $\text{Ca}^{2+}$  signalling post-vessel wounding,  
448 Erk-signalling is activated progressively in ECs closest to the wounded site first,  
449 followed by those further away.

450

## 451 **Discussion**

452 ERK-signalling is a downstream target for a number of pathways essential for  
453 development (including VEGFA/VEGFR2, EGF/EGFR, FGF/FGFR pathways) and  
454 plays a central role in organ development by promoting proliferation, growth,  
455 migration and differentiation (Hogan and Schulte-Merker, 2017;Lavoie et al., 2020).  
456 As such, Erk-signalling must be tightly regulated in both its spatial and temporal  
457 activation. To understand how dynamically Erk activity is regulated in developing  
458 vasculature, we generated the EC-EKC transgenic line and validated its use as a  
459 proxy readout of active Erk-signalling in vasculature. We found that it both provided a  
460 valid readout for physiological Erk-signalling and uncovered previously  
461 unappreciated Erk-signalling dynamics during vessel regeneration (**Figure 7**). In the  
462 context of tip cell proliferation in angiogenesis, we revealed very rapid post-cell  
463 division signalling asymmetry, confirming previous work based on static imaging  
464 (Costa et al., 2016). In regenerative angiogenesis, we reveal a two-step mechanism  
465 for Erk-signalling activation post-vessel wounding, that involves an immediate and an  
466 ongoing signalling response that progressively limits Erk-signalling to vessels that  
467 are regenerating. Importantly, this study shows the utility of this new transgenic line  
468 to elucidate dynamic Erk-signalling events in vertebrate ECs and we suggest it will  
469 be a useful tool for diverse future studies of development and disease.

470

471 At a technical level, we used various quantification methods for measuring Erk  
472 activity in ECs and all generated valid results. The ratio of nuclear/cytoplasm EKC  
473 localisation gives the most accurate readout (Regot et al., 2014), but can only be  
474 used when a cells cytoplasmic fluorescence can be accurately measured. This is  
475 especially challenging for ECs which overlap and have unpredictable morphology in  
476 vascular tubes. De la Cova and colleagues, used a second generation ERK KTR  
477 which includes a nuclear localised H2B-mCherry expressed from the same promoter,  
478 allowing them to quantify Erk activity based on the Clover/mCherry ratio in *C.*  
479 *elegans* (de la Cova et al., 2017). We used a similar approach here with two  
480 independent transgenes driving EKC and H2B-mCherry and produced highly  
481 consistent results. It is worth noting that inter-embryo/larvae variations in H2B-  
482 mCherry intensity need to be considered, hence transgenic lines that express both  
483 ERK KTR and H2B-mCherry under a single promoter would be ideal. Finally, we also  
484 used the measurement of nuclear EKC normalised to the average EKC intensity of  
485 the DA to normalise for embryo to embryo variation. This approach also provided  
486 data consistent with the other two methods. Thus, overall this EC-EKC model is  
487 highly robust with multiple methods to quantify and normalise sensor localisation. As  
488 KTR reporters are used more frequently *in vivo* in the future, the quantification  
489 methods used here may be applied to many scenarios analysing cellular Erk activity  
490 in cells with complex 3D morphology.

491

492 Studies in zebrafish and *Xenopus* have demonstrated rapid Erk activation in  
493 epithelial cells upon local wounding, which subsides relatively quickly (within 1hpa)  
494 as tissue repair progresses (Li et al., 2013;Mayr et al., 2018). Interestingly, our work  
495 shows a similar, very rapid, Erk activation in all vasculature in proximity of a wound.  
496 This suggests a common, initial, rapid Erk-signalling response immediately post-  
497 wounding in many different cell types and tissues – as if cells adjacent to a wound  
498 are rapidly primed to respond. However, in the vasculature this signalling returned to  
499 pre-ablation levels by 1 hpa, while Erk activity was maintained for a longer timeframe  
500 only in the wounded vessels. This ongoing, later signalling was maintained through  
501 Vegfr activity, likely stimulated in part by Vegfa secreted from macrophages  
502 (Gurevich et al., 2018) and our data suggests other local sources of Vegfs (see  
503 **Figure 7**). Thus, Erk-signalling dynamics between wounded (ablated) and

504 unwounded (adjacent) vessels differed significantly. We suggest this difference  
505 represents an initial priming of the wounded tissue (the rapid Erk response) that is  
506 replaced overtime with sustained vascular Erk-signalling that is essential in the  
507 regenerative response.

508

509 Rapid  $\text{Ca}^{2+}$  signalling post-wounding is observed in multiple systems *in vitro* and *in*  
510 *vivo* (reviewed in detail in (Ghilardi et al., 2020)). Using both quantitative live imaging  
511 and pharmacological inhibition, we found that  $\text{Ca}^{2+}$  signalling is required for Erk  
512 activation in ablated ISV ECs. Taking advantage of the high spatial and temporal  
513 resolution in our model, we found that  $\text{Ca}^{2+}$ -dependent Erk-signalling is activated  
514 progressively from cells closest to the wound to cells further away. This may be  
515 consistent with a wave of  $\text{Ca}^{2+}$  signalling through the wounded vessel. Activation of  
516 Erk-signalling at 2 mpa in wounded epithelial cells in *Xenopus* promotes actomyosin  
517 contraction and wound closure (Li et al., 2013). Therefore, rapid  $\text{Ca}^{2+}$  signalling-  
518 mediated Erk activation in the wounded vessel may ensure efficient wound closure in  
519 ablated ISVs. At a molecular mechanistic level, it seems likely that EC  $\text{Ca}^{2+}$   
520 signalling is influenced by either the activity of transient receptor potential (TRP)  
521 channels (Smani et al., 2018) or P2X receptors (P2X4 or P2X7) (Surprenant and  
522 North, 2009) which are active in ECs and can influence angiogenesis, cytoskeletal  
523 remodelling and vascular permeability. We found no evidence that  $\text{Ca}^{2+}$  signalling  
524 influenced the broader, rapid Erk-signalling response in unwounded but adjacent  
525 vasculature. One interesting candidate to contribute to this broader mechanism is  
526 altered tissue tension associated with the tissue ablation, which had been shown in  
527 some contexts to modulate ERK-signalling (Rosenfeldt and Grinnell, 2000; Hirata et  
528 al., 2015). Perhaps consistent with this idea, we did not identify a mechanism  
529 required for rapid Erk activation in adjacent ISV ECs and vessel wounding was not  
530 required - tissue wounding in between ISVs alone activated Erk-signalling in  
531 surrounding ECs. Further work is needed to fully appreciate the role of mechanical  
532 contributions in this response. Nevertheless, rapid Erk activation in ECs upon  
533 wounding seems likely to potentiate these ECs to more rapidly respond to external  
534 growth factors such as Vegfa upon the later activation of the inflammatory response  
535 and initiation of sustained regenerative angiogenesis.

536

537 Taking advantage of spatial information in the imaging data, we showed that ECs in  
538 wounded ISVs that are actively regenerating at 3 hpa display a graded signalling  
539 response along the vessel at the level of Vegfr/Erk activity. This is likely due to a  
540 local source (or sources) of Vegfa and may explain why unwounded ISV ECs, which  
541 are further away from the Vegfa source, do not sustain high Erk activity at 3 hpa. In  
542 bigger wounds, excessive angiogenesis has been previously reported to occur from  
543 adjacent ISVs and macrophage-dependent vascular regression is then required to  
544 ensure vessel patterns return to their original state (Gurevich et al., 2018). Therefore,  
545 we hypothesise that maintaining Erk activity only in ECs of vessels that need to  
546 regenerate in this laser ablation model, ensures EC proliferation and migration only  
547 occurs in regenerating vessels, and prevents excessive angiogenesis. Further  
548 studies could investigate Erk-signalling dynamics of ECs in bigger wounds, which  
549 more closely resemble traumatic injury in humans and could further assess Erk-  
550 signalling dynamics in excessive angiogenesis and regression.

551

552 Blood vessels constantly remodel to accommodate for the needs of the human body  
553 during development and disease (Carmeliet and Jain, 2011; Chung and Ferrara,  
554 2011; Potente et al., 2011). It is therefore not surprising that Erk-signalling, which is a  
555 key modulator of angiogenesis, is highly dynamic in ECs. As a novel tool that allows  
556 real-time analysis of Erk activity, EC-EKC biosensors will be useful for elucidating  
557 Erk-signalling events in vasculature in an array of settings and different vertebrate  
558 models. Importantly, in zebrafish the EC-EKC transgenic line can be coupled with  
559 both established and novel mutants with vascular phenotypes to investigate how  
560 real-time EC Erk-signalling dynamics is affected in the absence of key vascular  
561 genes. Further, dynamic Erk-signalling events in ECs in zebrafish disease models  
562 associated with increased angiogenesis such as in cancer (Nicoli et al., 2007) and  
563 tuberculosis (Oehlers et al., 2015) can be analysed using this EC-EKC model. This  
564 could highlight novel pathological Erk-signalling events in ECs, that could be  
565 normalised using drugs shown to modulate Erk-signalling (Goglia et al., 2020). Of  
566 note, KTR constructs for other kinases such as AKT, JNK and p38 are also now  
567 available (Regot et al., 2014; Maryu et al., 2016). Other types of fluorescence-based  
568 kinase activity reporters such as separation of phases-based activity reporter of  
569 kinases (SPARK), could also be applied (Zhang et al., 2018). Future studies will  
570 inevitably combine multiple signalling biosensors to elucidate real-time interactions

571 between signalling pathways as they decipher incoming signals and drive  
572 development and disease.



573 **Materials and methods**

574

575 **Key resources table**

576

Reagent type (species) or resource	Designation	Source or reference	Identifiers	Additional information/reagent source
Genetic reagent ( <i>D. rerio</i> )	<i>Tg(fli1a:H2B- mCherry)<sup>uq37bh</sup></i>	(Baek et al., 2019)	RRID:ZFIN_ZDB- ALT-191011-5	Ben M Hogan (Organogenesis and Cancer Program, Peter MacCallum Cancer Centre, Australia)
Genetic reagent ( <i>D. rerio</i> )	<i>Tg(fli1a:EGFP)<sup>y1</sup></i>	(Lawson and Weinstein, 2002)	RRID:ZFIN_ZDB- ALT-011017-8	Brant M Weinstein (National Institute of Child Health and Human Development, Bethesda, USA)
Genetic reagent ( <i>D. rerio</i> )	<i>Tg(fli1aep:ERK-KTR- Clover)<sup>uq39bh</sup></i>	This study		Ben M Hogan (Organogenesis and Cancer Program, Peter MacCallum Cancer Centre, Australia)
Genetic reagent ( <i>D. rerio</i> )	<i>Tg(ubb:Mmu.Elk1-KTR- mClover)<sup>vi1</sup></i>	(Mayr et al., 2018)	ZFIN ID: ZDB-ALT- 190211-6	Martin Distel (Children's Cancer Research Institute, Austria)
Genetic reagent ( <i>D. rerio</i> )	<i>Tg(actb2:GCaMP6f)<sup>zf3076</sup></i>	(Herzog et al., 2019)	ZFIN ID: ZDB-ALT- 200610-2	Leah Herrgen (Centre for Discovery Brain Sciences, University of Edinburgh, Germany)

Genetic reagent ( <i>D. rerio</i> )	<i>Tg(kdrl:mCherry-CAAX)<sup>y171</sup></i>	(Fujita et al., 2011)	RRID:ZFIN_ZDB-ALT-110429-3	Brent M Weinstein (National Institute of Child Health and Human Development, Bethesda, USA)
Genetic reagent ( <i>D. rerio</i> )	<i>Tg(mpeg1:mCherry)<sup>gl23</sup></i>	(Ellett et al., 2011)	RRID:ZFIN_ZDB-ALT-120117-2	Graham Lieschke (Australian Regenerative Medicine Institute, Monash University, Australia)
Genetic reagent ( <i>D. rerio</i> )	<i>Tg(kdrl:EGFP)<sup>s843</sup></i>	(Beis et al., 2005)	RRID:ZFIN_ZDB-ALT-050916-14	Didier Stainier (Max Planck Institute for Heart and Lung Research, Germany)
Sequence-based reagent	MO1-spi1b	(Rhodes et al., 2005)	ZFIN ID: ZDB-MRPHLNO-050224-1	Genetools, LLC, OR, USA
Sequence-based reagent	MO3-csf3r	(Ellett et al., 2011)	ZFIN ID: ZDB-MRPHLNO-111213-1	Genetools, LLC, OR, USA
Software, algorithm	FIJI	ImageJ ( <a href="http://imagej.nih.gov/ij/">http://imagej.nih.gov/ij/</a> )	RRID:SCR_002285	Image processing and analysis, Version Fiji version 1
Software, algorithm	Imaris x64	Bitplane, Belfast, UK	RRID:SCR_007370	Image processing and analysis, Version 9.5.1
Software, algorithm	GraphPad Prism	GraphPad Prism ( <a href="http://graphpad.com">http://graphpad.com</a> )	RRID:SCR_002798	Statistics, Prism8: Version 8.3.0

Software, algorithm	R/R Studio	R project (r- project.org)	RRID:SCR_001905	Statistics, R version 4.0.2
Chemical compound, drug	SL327 (MEK signalling inhibitor)	Merck, Darmstadt, Germany	S4069	Diluted in DMSO
Chemical compound, drug	Trametinib (MEK signalling inhibitor)	Selleck chemicals, TX, USA	S2673	Diluted in DMSO
Chemical compound, drug	SU5416	Merck, Darmstadt, Germany	S8442	Diluted in DMSO
Chemical compound, drug	AV951	Adooq Bioscience, CA, USA	475108-18-0	Diluted in DMSO
Chemical compound, drug	Nifedipine	Bio-Techne, MN, USA	1075	Diluted in DMSO
Chemical compound, drug	Amlodipine	Merck, Darmstadt, Germany	A5605	Diluted in DMSO

## 578 **Zebrafish**

579 All zebrafish work was conducted in accordance with the guidelines of the animal  
580 ethics committees at the University of Queensland (AE54297), University of  
581 Melbourne, Peter MacCallum Cancer Centre (E634 and E643), University of Bristol  
582 (3003318), and the Children's Cancer Research Institute (GZ:565304/2014/6 and  
583 GZ:534619/2014/4). The transgenic zebrafish lines used were published previously  
584 as following: *Tg(fli1a:H2B-mCherry)<sup>uq37bh</sup>* (Baek et al., 2019), *Tg(fli1a:EGFP)<sup>y1</sup>*  
585 (Lawson and Weinstein, 2002), *Tg(ubb:Mmu.Elk1-KTR-mClover)<sup>vi1</sup>* (Mayr et al.,  
586 2018), *Tg(actb2:GCaMP6f)<sup>zf3076</sup>* (Herzog et al., 2019), *Tg(kdrl:mCherry-CAAX)<sup>y171</sup>*  
587 (Fujita et al., 2011), *Tg(mpeg1:mCherry)<sup>gl23</sup>* (Ellett et al., 2011), and  
588 *Tg(kdrl:EGFP)<sup>s843</sup>* (Beis et al., 2005). The *Tg(fli1aep:ERK-KTR-Clover)<sup>uq39bh</sup>*  
589 transgenic line (referred to as *Tg(fli1aep:EKC)/EC-EKC* in this study) was generated  
590 for this study using Gateway cloning and transgenesis. The pENTR-ERKKTRClover  
591 plasmid (#59138) was purchased from Addgene.

592

## 593 **Live imaging and laser-inflicted vessel/tissue wounding**

594 Embryos/Larvae at indicated stages were immobilised with Tricaine (0.08 mg/ml)  
595 and mounted laterally in either 1.2% ultra-low gelling agarose (specifically for **Video**  
596 **6**), 0.25% low melting agarose (specifically for **Videos 7 and 8**, and **Figure 6A**), or  
597 0.5% low melting agarose (Merck, Darmstadt, Germany, A9414-100G) as previously  
598 described (Okuda et al., 2018). Images were taken at indicated timepoints/timeframe  
599 using either a Zeiss LSM 710 confocal microscope using either a Zeiss Plan  
600 Apochromat 10X objective (dry, N.A. 0.45, specifically for **Figure 1B-E**) or a Zeiss  
601 Plan Apochromat 20X objective (dry, N.A. 0.8, specifically for **Figure 3A,B**), Zeiss  
602 Elyra 780 confocal microscope using either a Zeiss Apochromat 10X objective (dry,  
603 N.A. 0.45, specifically for **Figure 5-figure supplement 1K,L**) or a Zeiss Plan  
604 Apochromat 40X objective (water, N.A. 1.1, specifically for **Figure 3-figure**  
605 **supplement 1A-B'**, **Figure 3-figure supplement 2H,I**, **Figure 5-figure supplement**  
606 **1M-T'**, **Figure 5-figure supplement 2A-H'**, and for **Figure 6-figure supplement 2I-**  
607 **N'**), Leica SP8 X WLL confocal microscope using a Leica HC PL APO CS2 40X  
608 objective (water, N.A. 1.1, specifically for **Video 6**), Leica TCS SP8 multiphoton  
609 microscope using a Leica HC Fluotar 25X objective (water, N.A. 0.95, specifically for  
610 **Videos 7 and 8**, and **Figure 6A**), Olympus Yokogawa CSU-W1 Spinning Disc  
611 Confocal microscope using a UPLSAPO 40X objective (silicon, N.A. 1.25,

612 specifically for **Figure 6-figure supplement 1K-T'**), or an Andor Dragonfly Spinning  
613 Disc Confocal microscope using a Nikon Apo  $\lambda$  LWD 40X objective (water, N.A.  
614 1.15).

615  
616 Muscle wounding in 30 hpf *Tg(ubb:Mmu.Elk1-KTR-mClover)* embryos were  
617 conducted as previously described (specifically for **Video 6**) (Mayr et al., 2018).  
618 Briefly, a laser-inflicted wound was introduced on mounted embryos using the Leica  
619 SP8 X FRAP module with the UV laser line of 405 nm at 85% laser power. Vessel  
620 wounding in 4 dpf *Tg(actb2:GCaMP6f);Tg(kdrl:mCherry-CAAX)* larvae were  
621 conducted as previously described (specifically for **Video 7 and 8**, and **Figure 6A**)  
622 (Gurevich et al., 2018). Briefly, a laser-inflicted wound was introduced on mounted  
623 larvae using a Micropoint laser (Spectra-Physics, CA, USA) connected to a Zeiss  
624 Axioplan II microscope with a laser pulse at a wavelength of 435 nm. All other  
625 tissue/vessel wounding in either 3 dpf (specifically for **Figure 3-figure supplement**  
626 **2B,C,H,I,P,R,T,V** and **Figure 5-figure supplement 2F,H**) or 4 dpf  
627 *Tg(fli1aep:EKC);Tg(fli1a:H2B-mCherry)* or *Tg(kdrl:EGFP);Tg(mpeg1:mCherry)*  
628 larvae were conducted using either a Zeiss LSM 710 confocal microscope or a  
629 Olympus FVMPE-RS multiphoton microscope. Briefly, a laser-inflicted wound was  
630 introduced on mounted larvae using a two-photon laser at 790 nm (Zeiss LSM 710  
631 confocal microscope) or 900 nm (Olympus FVMPE-RS multiphoton microscope) at  
632 80% laser power (Mai Tai, Spectra-Physics, CA, USA). The area of laser ablation for  
633 vessel wounding experiments was made consistent for all experiments (height: 40  
634  $\mu\text{m}$ , width: 15  $\mu\text{m}$ ). All vessel wounding was conducted on the ISV dorsal to the  
635 cloaca.

636  
637 For **Video 1**, time-lapse images of ISVs in 24-25 *Tg(fli1aep:EKC);Tg(fli1a:H2B-*  
638 *mCherry)* embryos were acquired every 14-17 seconds for 40 minutes using an  
639 Andor Dragonfly Spinning Disc Confocal microscope. Difference in time intervals  
640 were due to difference in z section number in different embryos. Pre-division ISV tip  
641 ECs with cytoplasmic H2B-mCherry localisation were selected for imaging. For  
642 **Videos 3-5**, time-lapse images of ISVs in 4 dpf *Tg(fli1aep:EKC);Tg(fli1a:H2B-*  
643 *mCherry)* larvae were taken every minute for 20 minutes using an Andor Dragonfly  
644 Spinning Disc Confocal microscope, wounded as described above using a Zeiss

645 LSM 710 confocal microscope, transferred to an Andor Dragonfly Spinning Disc  
646 Confocal microscope (allowing for 2 minutes to transfer the larvae and initiate  
647 imaging) and re-imaged every minute for another 20 minutes. As a control (**Video 2**),  
648 time-lapse images of ISVs in 4 dpf *Tg(fli1aep:EKC);Tg(fli1a:H2B-mCherry)* larvae  
649 were taken every minute for 41 minutes. For **Video 6**, time-lapse images of the trunk  
650 in a 30 hpf *Tg(ubb:Mmu.Elk1-KTR-mCherry)* embryo were acquired every 21  
651 minutes from 5 mpa until 3 hpa using a Leica SP8 X WLL confocal microscope. For  
652 **Video 8**, time-lapse images of ISVs in 4 dpf *Tg(actb2:GCaMP6f);Tg(kdrl:mCherry-*  
653 *CAAX)* larvae were acquired every minute from 5 mpa until 20 mpa using a Leica  
654 SP8 confocal microscope. As a control (**Video 7**), time-lapse images of ISVs in 4 dpf  
655 *Tg(actb2:GCaMP6f);Tg(kdrl:mCherry-CAAX)* larvae were acquired every minute for  
656 15 minutes using a Leica SP8 confocal microscope.

657

### 658 **Morpholino injections**

659 The *spi1b* and *csf3r* morpholinos used in this study have been validated and  
660 described previously (Rhodes et al., 2005;Ellett et al., 2011;Pase et al., 2012). A  
661 cocktail of *spi1b* (5ng) and *csf3r* (2.5ng) morpholinos were injected into 1-4 cell stage  
662 EC-*Tg(fli1aep:EKC);Tg(fli1a:H2B-mCherry)* or *Tg(mpeg1:mCherry)* embryos as  
663 previously described (Pase et al., 2012). ISVs of 3 dpf morphants/uninjected controls  
664 were imaged before vessel wounding, wounded as described above, and reimaged  
665 either at 15 mpa or at 3 hpa. To measure vessel regeneration, ISVs of 3 dpf  
666 morphants/uninjected controls were wounded as described above and imaged at 24  
667 hpa. Non-ablated 3 dpf *Tg(fli1aep:EKC);Tg(fli1a:H2B-mCherry)*  
668 morphants/uninjected controls were imaged, and re-imaged either 15 minutes or 3  
669 hours later. Macrophage numbers (*mpeg1:mCherry*-positive) in 3 dpf embryos  
670 (**Figure 3-figure supplement 2E,F**) or 4 dpf larvae (**Figure 3-figure supplement**  
671 **2A-C**) were manually quantified using the cell counter tool in FIJI.

672

### 673 **Drug treatments**

674 For investigating Erk activity in ISV tip ECs in 28 hpf embryos following drug  
675 treatment, 27 hpf *Tg(fli1aep:EKC);Tg(fli1a:H2B-mCherry)* embryos were treated for  
676 an hour with either 0.5% DMSO (vehicle control), 15  $\mu$ M SL327, 4  $\mu$ M SU5416, or  
677 500 nM AV951 diluted in E3 medium with 0.003% 1-phenyl-2-thiourea (PTU) and

678 imaged as described above at 28 hpf. Up to 5 ISV tip ECs were quantified per  
679 embryo.

680 For investigating the role of prolonged EC Erk activity in vessel regeneration, ISVs of  
681 4 dpf *Tg(fli1aep:EKC);Tg(fli1a:H2B-mCherry)* larvae were wounded as described  
682 above and were treated with either 0.5% DMSO (vehicle control), 4  $\mu$ M SU5416, 15  
683  $\mu$ M SL327, or 1  $\mu$ M Trametinib for 24 hours and imaged as described above at 5 dpf  
684 (24 hpa). For measuring Erk activity in ECs pre- and post-ablation in 4 dpf larvae  
685 following drug treatment, 4 dpf *Tg(fli1aep:EKC);Tg(fli1a:H2B-mCherry)* larvae were  
686 first treated for an hour with either 0.5% DMSO, 15  $\mu$ M SL327, 4  $\mu$ M or 10  $\mu$ M  
687 SU5416, or 500 nM AV951. ISVs of these larvae were imaged then wounded as  
688 described above in the presence of respective drugs at indicated concentrations in  
689 the mounting media. The same larvae were reimaged at 15 mpa. Alternatively,  
690 larvae were removed from mounting media following vessel wounding and incubated  
691 in respective drugs at indicated concentrations in E3 media, before being remounted  
692 and imaged at 3 hpa.

693 For Nifedipine and Amlodipine treatment, 4 dpf *Tg(fli1aep:EKC);Tg(fli1a:H2B-*  
694 *mCherry)* larvae were first treated for 30 minutes with either 1% DMSO, 50  $\mu$ M  
695 Nifedipine, or 100  $\mu$ M Amlodipine. This was because treatment for 1 hour with either  
696 50  $\mu$ M nifedipine or 100  $\mu$ M Amlodipine resulted in mortalities due to reduced cardiac  
697 function. The ISVs of these larvae were imaged and wounded as described above  
698 and reimaged 15 mpa. Alternatively, 4 dpf *Tg(fli1aep:EKC);Tg(fli1a:H2B-mCherry)*  
699 larvae were imaged before vessel wounding, and removed from mounting media  
700 following vessel wounding and incubated in 1% DMSO. 30 minutes before 3 hpa,  
701 larvae were treated with 50  $\mu$ M Nifedipine or continued its treatment with 1% DMSO,  
702 before being remounted in the presence of respective drugs at indicated  
703 concentrations and reimaged 3 hpa. To treat the larvae for 30 minutes with 50  $\mu$ M  
704 Nifedipine following vessel wounding, 4 dpf *Tg(fli1aep:EKC);Tg(fli1a:H2B-mCherry)*  
705 larvae were mounted with either 1% DMSO or 50  $\mu$ M Nifedipine, imaged before  
706 vessel wounding, and removed from mounting 30 minutes following vessel  
707 wounding. These larvae were incubated in 1% DMSO and reimaged 3 hpa. Non-  
708 ablated 4 dpf *Tg(fli1aep:EKC);Tg(fli1a:H2B-mCherry)* larvae controls were imaged,  
709 then reimaged either 15 minutes or 3 hours later.

710

## 711 **Guide RNA synthesis and injection**

712 *kdrl* guide RNA (gRNA) sequences were designed previously (Wu et al 2018). *Kdrl*

713 gRNA oligonucleotide 1:

714 TAATACGACTCACTATAGGCTTTCTGGTTCGATGGCAGTTTTAGAGCTAGAAATA

715 GC; *Kdrl* gRNA oligonucleotide 2:

716 TAATACGACTCACTATAGGCTGTAGAGACCCCTCTCCGTTTTAGAGCTAGAAAT

717 AGC; *Kdrl* gRNA oligonucleotide 3:

718 TAATACGACTCACTATAGGCACTCATAGCCGAGTGTAGTTTTAGAGCTAGAAAT

719 AGC; *Kdrl* gRNA oligonucleotide 4:

720 TAATACGACTCACTATAGGGTCACACTGCTCATCGAGTTTTAGAGCTAGAAAT

721 AGC. Guide RNAs were synthesised as described previously (Gagnon et al., 2014)

722 with modifications. Briefly, *kdrl* gRNA oligonucleotides were annealed to a constant

723 oligonucleotide, ssDNA overhangs were filled in with T4 DNA polymerase (New

724 England Biolabs, Victoria, Australia), and gRNA templates were purified using the

725 DNA Clean and Concentrator Kit (Zymo Research, D4014, CA, USA). *Kdrl* four-

726 guide RNA cocktail were transcribed with Ambion Megascript T7 promoter kit and

727 cleaned using the RNA clean and concentrator™ Kit (Zymo Research, R1014, CA,

728 USA). One-cell stage *Tg(fli1aep:EKC);Tg(fli1a:H2B-mCherry)* embryos were injected

729 with a cocktail of Cas9 protein (Integrated DNA Technologies, 1081059, IA, USA)

730 and the guide RNAs. Only *kdrl* crispants with clear vascular phenotypes (**Figure 5-**

731 **figure supplement 1L**) were used for all experiments. ISVs of 4 dpf

732 crispants/uninjected controls were imaged before vessel wounding, wounded as

733 described above, and reimaged at 3 hpa. Non-ablated 4 dpf

734 *Tg(fli1aep:EKC);Tg(fli1a:H2B-mCherry)* crispants/uninjected controls were imaged,

735 and re-imaged 3 hours later. As vessel wounding often resulted in no ECs in ISVs,

736 ECs from ablated connecting horizontal vessels were used for quantification (**Figure**

737 **5-figure supplement 1T**).

738

## 739 **Image processing and analysis**

740 Images were processed with image processing software FIJI version 1 (Schindelin et

741 al., 2012) and Imaris x64 (Bitplane, Version 9.5.1). Erk activity in ECs was measured

742 by either comparing nuclear/cytoplasm EKC intensity, nuclear EKC/H2B-mCherry

743 intensity, or nuclear EKC intensity. In Figures, EC-EKC intensity in nuclei is

744 represented after masking nuclear expression using H2B-mCherry and presenting



745 EC-EKC intensity in 16 colour LUT (Fiji). The nuclear/cytoplasm EKC intensity was  
746 quantified as described before (Kudo et al., 2018) with modifications, using a semi-  
747 autonomous custom written script in the ImageJ macro language. Briefly, z stack  
748 images were first processed into a maximum intensity z-projection. H2B-mCherry-  
749 positive EC nuclei underwent thresholding and were selected as individual regions of  
750 interest (ROI). The EKC channel was converted to a 32-bit image with background  
751 (non-cell associated) pixels converted to NaN. The average pixel intensity of EKC in  
752 the nuclei ROIs were measured (nuclear EKC intensity). Nuclei ROIs were then  
753 expanded and converted to a banded selection of the adjacent cytoplasmic area and  
754 the average pixel intensity of EKC within the expanded ROIs were measured  
755 (cytoplasm EKC intensity). The custom written ImageJ macro is available here:  
756 [\[https://github.com/NickCondon/Nuclei-Cyto\\_MeasuringScript\]](https://github.com/NickCondon/Nuclei-Cyto_MeasuringScript).

757

758 The average pixel intensity of either nuclear EKC or H2B-mCherry of ECs in 3D was  
759 quantified using Imaris software. The entire EC nucleus was masked using the H2B-  
760 mCherry signal. **Figure 2J and K** represent averages of data within each minute.  
761 For Embryos/larvae exposed to long-term time-lapse (for example **Videos 2-5**), or  
762 ablated with high-powered multiphoton laser for ablation studies, difference in  
763 photostability between fluorophores could significantly alter the ratio of nuclear  
764 EKC/H2B-mCherry intensity (Lam et al., 2012). Therefore, we either compared the  
765 ratio of nuclear EKC intensities between ECs within the same fish (for example  
766 **Video 1**), or we normalised EC nuclear EKC intensity with the average EKC intensity  
767 of another EKC-expressing structure (for example **Videos 2-5**). For larvae that  
768 underwent laser-inflicted wounding, nuclear EKC intensity pre- and post- ablation  
769 was normalised with the average pixel intensity of EKC of the entire DA within 2  
770 somite length. The ROI that covers the same DA region in pre- and post-wounded  
771 larvae was manually selected on a maximum intensity z-projection of the EKC  
772 channel, and average pixel intensity was calculated using FIJI. Datasets were  
773 presented as either the ratio of post/pre-ablation normalised nuclear EKC intensity,  
774 or as normalised nuclear EKC intensity further normalised to normalised nuclear  
775 EKC intensity in 2 mpa ECs (specifically for **Figure 6H**). 3 closest ECs from the  
776 wounded site in both ablated and adjacent ISVs were quantified, except for **Figures**  
777 **5I and 6H**, where 5 closest ECs from the wounded site in ablated ISVs were  
778 analysed. For **Videos 2-5**, reduction in EKC intensity due to photobleaching was

779 minimised using the bleach correction tool (correction method: Histogram Matching)  
780 in FIJI, however quantifications were all done using raw data.

781

782 GCaMP6f average pixel intensity on ISVs and unablated tissue in 4 dpf  
783 *Tg(actb2:GCaMP6f);Tg(kdrl:mCherry-CAAX)* larvae was measured using FIJI.  
784 Maximum intensity z-projection images of both GCaMP6f and mCherry-CAAX  
785 channels were first corrected for any drift in x/y dimensions. A ROI was drawn  
786 around the mCherry-CAAX-positive ISV segment nearest to the site of injury (an  
787 area consistently between 100-150  $\mu\text{m}^2$ ) and the average pixel intensity of GCaMP6f  
788 within the ROI at each timepoints were measured using FIJI. Similar measurements  
789 were acquired for adjacent ISVs, ISVs in unablated control larvae, and uninjured  
790 tissue, maintaining consistent size of ROI within each biological replicate. ISV  
791 GCaMP6f average pixel intensity was normalised to the average pixel intensity in  
792 uninjured tissue GCaMP6f within the same larvae.

793

794 The percentage of ISV height was measured by dividing the total horizontal height of  
795 the ISV with the prospective total horizontal height of the ISV (the horizontal height  
796 from the base ISV/DA intersection to the tip of the ISV/DLAV intersection. Ellipticity  
797 (elliptic) of ISV tip ECs were quantified using Imaris software. Original raw data with  
798 relevant acquisition metadata can be provided upon request.

799

## 800 **Statistics**

801 Graphic representations of data and statistical analysis was performed using either  
802 Prism 8 Version 8.3.0 or R software. Mann-Whitney test was conducted when  
803 comparing two datasets and Kruskal-Wallis test was conducted when comparing  
804 multiple datasets using Prism 8 (except for **Figure 5B**, which conducted an ordinary  
805 one-way ANOVA test, following confirmation of normality of all datasets using  
806 Anderson-Darling, D'Agostino and Pearson, Shapiro-Wilk, and Kolmogorov-Smirnov  
807 tests). Natural permutation test (**Figure 3H and Figure 4C**) or two-sample  
808 Kolmogorov-Smirnov test (**Figure 6H**) was used to test for differences between the  
809 population mean curve for datasets using R statistical software. For **Figure 6H**, we  
810 applied the non-parametric two sample Kolmogorov-Smirnov test to evaluate  
811 whether the distribution of Erk activity for each position differed from that of the

812 control. Null hypothesis was rejected where the D-statistic (maximum difference  
813 between two ECDF) exceeded the critical threshold (critical D) for each comparison  
814 and p-value < 0.001. D statistic indicates magnitude of change for each curve  
815 compared with control. Critical D varied for each position as follows: control vs 1<sup>st</sup> EC  
816 from wound, 0.166; control vs 2<sup>nd</sup> EC from wound, 0.166; control vs 3<sup>rd</sup> EC from  
817 wound, 0.166; control vs 4<sup>th</sup> EC from wound, 0.173; control vs 5<sup>th</sup> EC from wound,  
818 0.209. P-value below 0.05 was considered statistically significant for all data. Error  
819 bars in all graphs represent standard deviation.

820

### 821 **Acknowledgements**

822 This work was supported by NHMRC grants 1164734 and 1165117. BMH was  
823 supported by an NHMRC fellowship 1155221. We thank Dr Enid Lam for technical  
824 assistance. Imaging was performed in the Australian Cancer Research Foundation's  
825 Cancer Ultrastructure and Function Facility at IMB, Centre for Advanced Histology  
826 and Microscopy at Peter MacCallum Cancer Centre, Wolfson Bioimaging Facility at  
827 University of Bristol, and the Zebrafish platform Austria for preclinical drug screening  
828 at the Children's Cancer Research Institute supported by the Austrian Research  
829 Promotion Agency (FFG) project 7640628 (Danio4Can). We thank Olympus for use  
830 of the Olympus Yokogawa CSU-W1 Spinning Disc Confocal microscope.

831

832 **References**

- 833 Aoki, K., Kondo, Y., Naoki, H., Hiratsuka, T., Itoh, R.E., and Matsuda, M. (2017). Propagating  
834 Wave of ERK Activation Orients Collective Cell Migration. *Dev Cell* 43, 305-317 e305.
- 835 Baek, S., Oh, T.G., Secker, G., Sutton, D.L., Okuda, K.S., Paterson, S., Bower, N.I., Toubia, J.,  
836 Koltowska, K., Capon, S.J., Baillie, G.J., Simons, C., Muscat, G.E.O., Legendijk, A.K.,  
837 Smith, K.A., Harvey, N.L., and Hogan, B.M. (2019). The Alternative Splicing Regulator  
838 Nova2 Constrains Vascular Erk Signaling to Limit Specification of the Lymphatic  
839 Lineage. *Dev Cell* 49, 279-292 e275.
- 840 Beerman, R.W., Matty, M.A., Au, G.G., Looger, L.L., Choudhury, K.R., Keller, P.J., and Tobin,  
841 D.M. (2015). Direct In Vivo Manipulation and Imaging of Calcium Transients in  
842 Neutrophils Identify a Critical Role for Leading-Edge Calcium Flux. *Cell Rep* 13, 2107-  
843 2117.
- 844 Beis, D., Bartman, T., Jin, S.W., Scott, I.C., D'amico, L.A., Ober, E.A., Verkade, H., Frantsve, J.,  
845 Field, H.A., Wehman, A., Baier, H., Tallafuss, A., Bally-Cuif, L., Chen, J.N., Stainier,  
846 D.Y., and Jungblut, B. (2005). Genetic and cellular analyses of zebrafish  
847 atrioventricular cushion and valve development. *Development* 132, 4193-4204.
- 848 Berra-Romani, R., Raqeeb, A., Avelino-Cruz, J.E., Moccia, F., Oldani, A., Speroni, F., Taglietti,  
849 V., and Tanzi, F. (2008). Ca<sup>2+</sup> signaling in injured in situ endothelium of rat aorta. *Cell*  
850 *Calcium* 44, 298-309.
- 851 Berra-Romani, R., Raqeeb, A., Torres-Jacome, J., Guzman-Silva, A., Guerra, G., Tanzi, F., and  
852 Moccia, F. (2012). The mechanism of injury-induced intracellular calcium  
853 concentration oscillations in the endothelium of excised rat aorta. *J Vasc Res* 49, 65-  
854 76.
- 855 Carmeliet, P., and Jain, R.K. (2011). Molecular mechanisms and clinical applications of  
856 angiogenesis. *Nature* 473, 298-307.
- 857 Chang, C.I., Xu, B.E., Akella, R., Cobb, M.H., and Goldsmith, E.J. (2002). Crystal structures of  
858 MAP kinase p38 complexed to the docking sites on its nuclear substrate MEF2A and  
859 activator MKK3b. *Mol Cell* 9, 1241-1249.
- 860 Chia, K., Keatinge, M., Mazzolini, J., and Sieger, D. (2019). Brain tumours repurpose  
861 endogenous neuron to microglia signalling mechanisms to promote their own  
862 proliferation. *Elife* 8.
- 863 Chung, A.S., and Ferrara, N. (2011). Developmental and pathological angiogenesis. *Annu Rev*  
864 *Cell Dev Biol* 27, 563-584.
- 865 Costa, G., Harrington, K.I., Lovegrove, H.E., Page, D.J., Chakravartula, S., Bentley, K., and  
866 Herbert, S.P. (2016). Asymmetric division coordinates collective cell migration in  
867 angiogenesis. *Nat Cell Biol* 18, 1292-1301.
- 868 Covassin, L.D., Villefranc, J.A., Kacergis, M.C., Weinstein, B.M., and Lawson, N.D. (2006).  
869 Distinct genetic interactions between multiple Vegf receptors are required for  
870 development of different blood vessel types in zebrafish. *Proc Natl Acad Sci U S A*  
871 103, 6554-6559.
- 872 De La Cova, C., Townley, R., Regot, S., and Greenwald, I. (2017). A Real-Time Biosensor for  
873 ERK Activity Reveals Signaling Dynamics during *C. elegans* Cell Fate Specification. *Dev*  
874 *Cell* 42, 542-553 e544.
- 875 De Oliveira, S., Lopez-Munoz, A., Candel, S., Pelegrin, P., Calado, A., and Mulero, V. (2014).  
876 ATP modulates acute inflammation in vivo through dual oxidase 1-derived H<sub>2</sub>O<sub>2</sub>  
877 production and NF-kappaB activation. *J Immunol* 192, 5710-5719.

878 De Simone, A., Evanitsky, M.N., Hayden, L., Cox, B.D., Wang, J., Tornini, V.A., Ou, J., Chao, A.,  
879 Poss, K.D., and Di Talia, S. (2021). Control of osteoblast regeneration by a train of Erk  
880 activity waves. *Nature* 590, 129-133.

881 Deng, Y., Atri, D., Eichmann, A., and Simons, M. (2013). Endothelial ERK signaling controls  
882 lymphatic fate specification. *J Clin Invest* 123, 1202-1215.

883 Ding, Y., Li, J., Enterina, J.R., Shen, Y., Zhang, I., Tewson, P.H., Mo, G.C., Zhang, J., Quinn,  
884 A.M., Hughes, T.E., Maysinger, D., Alford, S.C., Zhang, Y., and Campbell, R.E. (2015).  
885 Ratiometric biosensors based on dimerization-dependent fluorescent protein  
886 exchange. *Nat Methods* 12, 195-198.

887 Ellett, F., Pase, L., Hayman, J.W., Andrianopoulos, A., and Lieschke, G.J. (2011). mpeg1  
888 promoter transgenes direct macrophage-lineage expression in zebrafish. *Blood* 117,  
889 e49-56.

890 Fujita, M., Cha, Y.R., Pham, V.N., Sakurai, A., Roman, B.L., Gutkind, J.S., and Weinstein, B.M.  
891 (2011). Assembly and patterning of the vascular network of the vertebrate  
892 hindbrain. *Development* 138, 1705-1715.

893 Gagnon, J.A., Valen, E., Thyme, S.B., Huang, P., Akhmetova, L., Pauli, A., Montague, T.G.,  
894 Zimmerman, S., Richter, C., and Schier, A.F. (2014). Efficient mutagenesis by Cas9  
895 protein-mediated oligonucleotide insertion and large-scale assessment of single-  
896 guide RNAs. *PLoS One* 9, e98186.

897 Ghilardi, S.J., O'reilly, B.M., and Sgro, A.E. (2020). Intracellular signaling dynamics and their  
898 role in coordinating tissue repair. *Wiley Interdiscip Rev Syst Biol Med* 12, e1479.

899 Goglia, A.G., Wilson, M.Z., Jena, S.G., Silbert, J., Basta, L.P., Devenport, D., and Toettcher,  
900 J.E. (2020). A Live-Cell Screen for Altered Erk Dynamics Reveals Principles of  
901 Proliferative Control. *Cell Syst* 10, 240-253 e246.

902 Goto, A., Nakahara, I., Yamaguchi, T., Kamioka, Y., Sumiyama, K., Matsuda, M., Nakanishi, S.,  
903 and Funabiki, K. (2015). Circuit-dependent striatal PKA and ERK signaling underlies  
904 rapid behavioral shift in mating reaction of male mice. *Proc Natl Acad Sci U S A* 112,  
905 6718-6723.

906 Gurevich, D.B., Severn, C.E., Twomey, C., Greenhough, A., Cash, J., Toye, A.M., Mellor, H.,  
907 and Martin, P. (2018). Live imaging of wound angiogenesis reveals macrophage  
908 orchestrated vessel sprouting and regression. *EMBO J* 37.

909 Habeck, H., Odenthal, J., Walderich, B., Maischein, H., Schulte-Merker, S., and Tübingen  
910 Screen, C. (2002). Analysis of a zebrafish VEGF receptor mutant reveals specific  
911 disruption of angiogenesis. *Curr Biol* 12, 1405-1412.

912 Handly, L.N., Pilko, A., and Wollman, R. (2015). Paracrine communication maximizes cellular  
913 response fidelity in wound signaling. *Elife* 4, e09652.

914 Harvey, C.D., Ehrhardt, A.G., Cellurale, C., Zhong, H., Yasuda, R., Davis, R.J., and Svoboda, K.  
915 (2008). A genetically encoded fluorescent sensor of ERK activity. *Proc Natl Acad Sci U*  
916 *S A* 105, 19264-19269.

917 Herzog, C., Pons Garcia, L., Keatinge, M., Greenald, D., Moritz, C., Peri, F., and Herrgen, L.  
918 (2019). Rapid clearance of cellular debris by microglia limits secondary neuronal cell  
919 death after brain injury in vivo. *Development* 146.

920 Hirata, H., Gupta, M., Vedula, S.R., Lim, C.T., Ladoux, B., and Sokabe, M. (2015). Actomyosin  
921 bundles serve as a tension sensor and a platform for ERK activation. *EMBO Rep* 16,  
922 250-257.

923 Hiratsuka, T., Fujita, Y., Naoki, H., Aoki, K., Kamioka, Y., and Matsuda, M. (2015). Intercellular  
924 propagation of extracellular signal-regulated kinase activation revealed by in vivo  
925 imaging of mouse skin. *Elife* 4, e05178.

926 Hogan, B.M., and Schulte-Merker, S. (2017). How to Plumb a Pisces: Understanding Vascular  
927 Development and Disease Using Zebrafish Embryos. *Dev Cell* 42, 567-583.

928 Kamioka, Y., Sumiyama, K., Mizuno, R., Sakai, Y., Hirata, E., Kiyokawa, E., and Matsuda, M.  
929 (2012). Live imaging of protein kinase activities in transgenic mice expressing FRET  
930 biosensors. *Cell Struct Funct* 37, 65-73.

931 Kamioka, Y., Takakura, K., Sumiyama, K., and Matsuda, M. (2017). Intravital Forster  
932 resonance energy transfer imaging reveals osteopontin-mediated  
933 polymorphonuclear leukocyte activation by tumor cell emboli. *Cancer Sci* 108, 226-  
934 235.

935 Koch, S., and Claesson-Welsh, L. (2012). Signal transduction by vascular endothelial growth  
936 factor receptors. *Cold Spring Harb Perspect Med* 2, a006502.

937 Komatsu, N., Aoki, K., Yamada, M., Yukinaga, H., Fujita, Y., Kamioka, Y., and Matsuda, M.  
938 (2011). Development of an optimized backbone of FRET biosensors for kinases and  
939 GTPases. *Mol Biol Cell* 22, 4647-4656.

940 Kudo, T., Jeknic, S., Macklin, D.N., Akhter, S., Hughey, J.J., Regot, S., and Covert, M.W.  
941 (2018). Live-cell measurements of kinase activity in single cells using translocation  
942 reporters. *Nat Protoc* 13, 155-169.

943 Lam, A.J., St-Pierre, F., Gong, Y., Marshall, J.D., Cranfill, P.J., Baird, M.A., Mckeown, M.R.,  
944 Wiedenmann, J., Davidson, M.W., Schnitzer, M.J., Tsien, R.Y., and Lin, M.Z. (2012).  
945 Improving FRET dynamic range with bright green and red fluorescent proteins. *Nat*  
946 *Methods* 9, 1005-1012.

947 Lavoie, H., Gagnon, J., and Therrien, M. (2020). ERK signalling: a master regulator of cell  
948 behaviour, life and fate. *Nat Rev Mol Cell Biol*.

949 Lawson, N.D., and Weinstein, B.M. (2002). In vivo imaging of embryonic vascular  
950 development using transgenic zebrafish. *Dev Biol* 248, 307-318.

951 Li, J., Zhang, S., Soto, X., Woolner, S., and Amaya, E. (2013). ERK and phosphoinositide 3-  
952 kinase temporally coordinate different modes of actin-based motility during  
953 embryonic wound healing. *J Cell Sci* 126, 5005-5017.

954 Maryu, G., Matsuda, M., and Aoki, K. (2016). Multiplexed Fluorescence Imaging of ERK and  
955 Akt Activities and Cell-cycle Progression. *Cell Struct Funct* 41, 81-92.

956 Matsubayashi, Y., Ebisuya, M., Honjoh, S., and Nishida, E. (2004). ERK activation propagates  
957 in epithelial cell sheets and regulates their migration during wound healing. *Curr Biol*  
958 14, 731-735.

959 Mayr, V., Sturtzel, C., Stadler, M., Grissenberger, S., and Distel, M. (2018). Fast Dynamic in  
960 vivo Monitoring of Erk Activity at Single Cell Resolution in DREKA Zebrafish. *Front Cell*  
961 *Dev Biol* 6, 111.

962 Mehta, S., Zhang, Y., Roth, R.H., Zhang, J.F., Mo, A., Tenner, B., Haganir, R.L., and Zhang, J.  
963 (2018). Single-fluorophore biosensors for sensitive and multiplexed detection of  
964 signalling activities. *Nat Cell Biol* 20, 1215-1225.

965 Mizuno, R., Kamioka, Y., Kabashima, K., Imajo, M., Sumiyama, K., Nakasho, E., Ito, T.,  
966 Hamazaki, Y., Okuchi, Y., Sakai, Y., Kiyokawa, E., and Matsuda, M. (2014). In vivo  
967 imaging reveals PKA regulation of ERK activity during neutrophil recruitment to  
968 inflamed intestines. *J Exp Med* 211, 1123-1136.

969 Moccia, F., Berra-Romani, R., and Tanzi, F. (2012). Update on vascular endothelial Ca(2+  
970 signalling: A tale of ion channels, pumps and transporters. *World J Biol Chem* 3, 127-  
971 158.

972 Murphy, D.A., Makonnen, S., Lassoued, W., Feldman, M.D., Carter, C., and Lee, W.M. (2006).  
973 Inhibition of tumor endothelial ERK activation, angiogenesis, and tumor growth by  
974 sorafenib (BAY43-9006). *Am J Pathol* 169, 1875-1885.

975 Nagasawa-Masuda, A., and Terai, K. (2016). ERK activation in endothelial cells is a novel  
976 marker during neovascuogenesis. *Genes Cells* 21, 1164-1175.

977 Nicoli, S., Ribatti, D., Cotelli, F., and Presta, M. (2007). Mammalian tumor xenografts induce  
978 neovascularization in zebrafish embryos. *Cancer Res* 67, 2927-2931.

979 Oehlers, S.H., Cronan, M.R., Scott, N.R., Thomas, M.I., Okuda, K.S., Walton, E.M., Beerman,  
980 R.W., Crosier, P.S., and Tobin, D.M. (2015). Interception of host angiogenic signalling  
981 limits mycobacterial growth. *Nature* 517, 612-615.

982 Okuda, K.S., Baek, S., and Hogan, B.M. (2018). Visualization and Tools for Analysis of  
983 Zebrafish Lymphatic Development. *Methods Mol Biol* 1846, 55-70.

984 Pase, L., Layton, J.E., Wittmann, C., Ellett, F., Nowell, C.J., Reyes-Aldasoro, C.C., Varma, S.,  
985 Rogers, K.L., Hall, C.J., Keightley, M.C., Crosier, P.S., Grabher, C., Heath, J.K.,  
986 Renshaw, S.A., and Lieschke, G.J. (2012). Neutrophil-delivered myeloperoxidase  
987 dampens the hydrogen peroxide burst after tissue wounding in zebrafish. *Curr Biol*  
988 22, 1818-1824.

989 Pokrass, M.J., Ryan, K.A., Xin, T., Pielstick, B., Timp, W., Greco, V., and Regot, S. (2020). Cell-  
990 Cycle-Dependent ERK Signaling Dynamics Direct Fate Specification in the Mammalian  
991 Preimplantation Embryo. *Dev Cell* 55, 328-340 e325.

992 Poplimont, H., Georgantzoglou, A., Boulch, M., Walker, H.A., Coombs, C.,  
993 Papaleonidopoulou, F., and Sarris, M. (2020). Neutrophil Swarming in Damaged  
994 Tissue Is Orchestrated by Connexins and Cooperative Calcium Alarm Signals. *Curr*  
995 *Biol* 30, 2761-2776 e2767.

996 Potente, M., Gerhardt, H., and Carmeliet, P. (2011). Basic and therapeutic aspects of  
997 angiogenesis. *Cell* 146, 873-887.

998 Razzell, W., Evans, I.R., Martin, P., and Wood, W. (2013). Calcium flashes orchestrate the  
999 wound inflammatory response through DUOX activation and hydrogen peroxide  
1000 release. *Curr Biol* 23, 424-429.

1001 Regot, S., Hughey, J.J., Bajar, B.T., Carrasco, S., and Covert, M.W. (2014). High-sensitivity  
1002 measurements of multiple kinase activities in live single cells. *Cell* 157, 1724-1734.

1003 Rhodes, J., Hagen, A., Hsu, K., Deng, M., Liu, T.X., Look, A.T., and Kanki, J.P. (2005). Interplay  
1004 of pu.1 and gata1 determines myelo-erythroid progenitor cell fate in zebrafish. *Dev*  
1005 *Cell* 8, 97-108.

1006 Ricard, N., Scott, R.P., Booth, C.J., Velazquez, H., Cilfone, N.A., Baylon, J.L., Gulcher, J.R.,  
1007 Quaggin, S.E., Chittenden, T.W., and Simons, M. (2019). Endothelial ERK1/2 signaling  
1008 maintains integrity of the quiescent endothelium. *J Exp Med* 216, 1874-1890.

1009 Rosenfeldt, H., and Grinnell, F. (2000). Fibroblast quiescence and the disruption of ERK  
1010 signaling in mechanically unloaded collagen matrices. *J Biol Chem* 275, 3088-3092.

1011 Sano, T., Kobayashi, T., Ogawa, O., and Matsuda, M. (2018). Gliding Basal Cell Migration of  
1012 the Urothelium during Wound Healing. *Am J Pathol* 188, 2564-2573.

1013 Schindelin, J., Arganda-Carreras, I., Frise, E., Kaynig, V., Longair, M., Pietzsch, T., Preibisch, S.,  
1014 Rueden, C., Saalfeld, S., Schmid, B., Tinevez, J.Y., White, D.J., Hartenstein, V., Eliceiri,

1015 K., Tomancak, P., and Cardona, A. (2012). Fiji: an open-source platform for biological-  
1016 image analysis. *Nat Methods* 9, 676-682.

1017 Shin, M., Beane, T.J., Quillien, A., Male, I., Zhu, L.J., and Lawson, N.D. (2016a). Vegfa signals  
1018 through ERK to promote angiogenesis, but not artery differentiation. *Development*  
1019 143, 3796-3805.

1020 Shin, M., Male, I., Beane, T.J., Villefranc, J.A., Kok, F.O., Zhu, L.J., and Lawson, N.D. (2016b).  
1021 Vegfc acts through ERK to induce sprouting and differentiation of trunk lymphatic  
1022 progenitors. *Development* 143, 3785-3795.

1023 Shu, X. (2020). Imaging dynamic cell signaling in vivo with new classes of fluorescent  
1024 reporters. *Curr Opin Chem Biol* 54, 1-9.

1025 Simons, M., Gordon, E., and Claesson-Welsh, L. (2016). Mechanisms and regulation of  
1026 endothelial VEGF receptor signalling. *Nat Rev Mol Cell Biol* 17, 611-625.

1027 Smani, T., Gomez, L.J., Regodon, S., Woodard, G.E., Siegfried, G., Khatib, A.M., and Rosado,  
1028 J.A. (2018). TRP Channels in Angiogenesis and Other Endothelial Functions. *Front*  
1029 *Physiol* 9, 1731.

1030 Srinivasan, R., Zabuawala, T., Huang, H., Zhang, J., Gulati, P., Fernandez, S., Karlo, J.C.,  
1031 Landreth, G.E., Leone, G., and Ostrowski, M.C. (2009). Erk1 and Erk2 regulate  
1032 endothelial cell proliferation and migration during mouse embryonic angiogenesis.  
1033 *PLoS One* 4, e8283.

1034 Surprenant, A., and North, R.A. (2009). Signaling at purinergic P2X receptors. *Annu Rev*  
1035 *Physiol* 71, 333-359.

1036 Takeda, H., and Kiyokawa, E. (2017). Activation of Erk in ileal epithelial cells engaged in  
1037 ischemic-injury repair. *Sci Rep* 7, 16469.

1038 Tang, S., and Yasuda, R. (2017). Imaging ERK and PKA Activation in Single Dendritic Spines  
1039 during Structural Plasticity. *Neuron* 93, 1315-1324 e1313.

1040 Villefranc, J.A., Amigo, J., and Lawson, N.D. (2007). Gateway compatible vectors for analysis  
1041 of gene function in the zebrafish. *Dev Dyn* 236, 3077-3087.

1042 Wilhelm, S.M., Carter, C., Tang, L., Wilkie, D., Mcnabola, A., Rong, H., Chen, C., Zhang, X.,  
1043 Vincent, P., Mchugh, M., Cao, Y., Shujath, J., Gawlak, S., Eveleigh, D., Rowley, B., Liu,  
1044 L., Adnane, L., Lynch, M., Auclair, D., Taylor, I., Gedrich, R., Voznesensky, A., Riedl, B.,  
1045 Post, L.E., Bollag, G., and Trail, P.A. (2004). BAY 43-9006 exhibits broad spectrum oral  
1046 antitumor activity and targets the RAF/MEK/ERK pathway and receptor tyrosine  
1047 kinases involved in tumor progression and angiogenesis. *Cancer Res* 64, 7099-7109.

1048 Wong, K.L., Akiyama, R., Bessho, Y., and Matsui, T. (2018). ERK Activity Dynamics during  
1049 Zebrafish Embryonic Development. *Int J Mol Sci* 20.

1050 Wu, R.S., Lam, Ii, Clay, H., Duong, D.N., Deo, R.C., and Coughlin, S.R. (2018). A Rapid Method  
1051 for Directed Gene Knockout for Screening in G0 Zebrafish. *Dev Cell* 46, 112-125 e114.

1052 Xiao, Z., Wang, T., Qin, H., Huang, C., Feng, Y., and Xia, Y. (2011). Endoplasmic reticulum  
1053 Ca<sup>2+</sup> release modulates endothelial nitric-oxide synthase via extracellular signal-  
1054 regulated kinase (ERK) 1/2-mediated serine 635 phosphorylation. *J Biol Chem* 286,  
1055 20100-20108.

1056 Yokota, Y., Nakajima, H., Wakayama, Y., Muto, A., Kawakami, K., Fukuhara, S., and  
1057 Mochizuki, N. (2015). Endothelial Ca<sup>2+</sup> oscillations reflect VEGFR signaling-regulated  
1058 angiogenic capacity in vivo. *Elife* 4.

1059 Yoo, S.K., Freisinger, C.M., Lebert, D.C., and Huttenlocher, A. (2012). Early redox, Src family  
1060 kinase, and calcium signaling integrate wound responses and tissue regeneration in  
1061 zebrafish. *J Cell Biol* 199, 225-234.



1062 Zhang, Q., Huang, H., Zhang, L., Wu, R., Chung, C.I., Zhang, S.Q., Torra, J., Schepis, A.,  
1063 Coughlin, S.R., Kornberg, T.B., and Shu, X. (2018). Visualizing Dynamics of Cell  
1064 Signaling In Vivo with a Phase Separation-Based Kinase Reporter. *Mol Cell* 69, 334-  
1065 346 e334.  
1066  
1067

1068 **Figures and figure legends**

1069

1070 **Figure 1: The EC-EKC transgenic line enables quantification of vascular Erk**  
1071 **activity during development.**

1072 (A) Schematic representation of the *fli1aep:ERK-KTR-Clover* (EKC) construct, and  
1073 ECs with nuclear enriched EKC (bottom left, inactive Erk-signalling) and nuclear  
1074 depleted EKC localisation (bottom right, active Erk-signalling).

1075 (B-E) Lateral confocal images of the EC-EKC (B,D) and *Tg(fli1a:EGFP)* (C,E)  
1076 embryos/larvae at 24 hpf (B,C) and 5 dpf (D,E). Blood vessel development is not  
1077 altered in EC-EKC embryos/larvae.

1078 (F-H'') Lateral spinning disc confocal images of ISV ECs in 28 hpf EC-EKC embryos  
1079 treated for 1 hour with either 0.5% DMSO (F-F''), with active EC Erk-signalling; or 15  
1080  $\mu$ M SL327 (G-G''), or 4  $\mu$ M SU5416 (H-H''); all of which with inactive EC Erk-  
1081 signalling. Images F-H show the *fli1aep:EKC* expression, while images F'-H' show  
1082 both the *fli1aep:EKC* and the *fli1a:H2B-mCherry* expression. Images F''-H'' show the  
1083 nuclear *fli1aep:EKC* expression with intensity difference represented in 16 colour  
1084 LUT (Fiji). The *fli1a:H2B-mCherry* signal was used to mask the nucleus.

1085 (I) Quantification of nucleus/cytoplasm EKC intensity in ISV tip ECs of 28 hpf  
1086 embryos treated with either 0.5% DMSO (0.881, 93 ISV tip ECs, n=20 embryos), 15  
1087  $\mu$ M SL327 (1.419, 114 ISV tip ECs, n=27 embryos), or 4  $\mu$ M SU5416 (1.591, 118  
1088 ISV tip ECs, n=27 embryos).

1089 ISV: intersegmental vessel. Statistical test: Kruskal Wallis test was conducted for  
1090 graph I. Error bars represent standard deviation. Scale bars: 200  $\mu$ m for images B  
1091 and D, 25  $\mu$ m for image F.

1092

1093 **Figure 2: Tip cells show asymmetric Erk activity immediately following cell**  
1094 **division.**

1095 (A-I) Still images from **Video 1** showing ISV ECs in a 24-25 hpf EC-EKC embryo at  
1096 indicated time points. The tip daughter cell has higher Erk activity when compared to  
1097 the stalk daughter cell immediately after cell division. Left panels show *fli1aep:EKC*  
1098 expression, middle panels show the *fli1a:H2B-mCherry* expression, and right panels  
1099 show the nuclear *fli1aep:EKC* intensity. The *fli1a:H2B-mCherry* signal was used to  
1100 mask the nucleus. The yellow arrow indicates a tip ISV EC with cytoplasmic  
1101 *fli1a:H2B-mCherry* expression. The light blue arrow indicates a tip ISV EC that has  
1102 undergone cytokinesis.

1103 (J,K) Quantification of tip/stalk nuclear EKC intensity of daughter ECs post-  
1104 cytokinesis (14 EC division events, n=14 embryos). Graph J shows quantification of  
1105 individual biological replicates and graph K shows the average of all biological  
1106 replicates.

1107 ISV: intersegmental vessel; DA: dorsal aorta. Error bars represent standard  
1108 deviation. Scale bar: 25  $\mu$ m.

1109

1110 **Figure 3: Wounded vessels rapidly activate Erk independent of macrophages**  
1111 **or Vegfr-signalling.**

1112 (A,B) Lateral confocal images of a 4 dpf *Tg(kdrl:EGFP)* larva following vessel  
1113 wounding (post-ablation). Image A shows the *kdrl:EGFP* expression and image B  
1114 shows the trans-light image of image A. Ablated ISV, adjacent ISVs, wounded site  
1115 indicated with white arrows.

1116 (C) Schematic representation of imaging schedule for larvae in images D-G and  
1117 **Videos 3-5.**

1118 (D-G') Still images from **Video 4** (D-E') and **Video 5** (F-G') showing ISV ECs before  
1119 (pre-ablation) and after vessel wounding. Ablated and adjacent ISV ECs rapidly  
1120 activate Erk-signalling. D-G = *fli1aep:EKC* expression, D'-G' = nuclear intensity.

1121 (H,I) Quantification of post/pre-ablation nuclear EKC intensity of ECs in non-ablated  
1122 control ISVs (black, 24 ECs, n=8 larvae), ablated ISVs (red, 27 ECs, n=9 larvae),  
1123 and adjacent ISVs (light blue, 27 ECs, n=9 larvae). H shows quantification of  
1124 individual ECs, I shows the average of all biological replicates. Green dotted line  
1125 indicates 15 minutes post-ablation (mpa).

1126 (J) Quantification of post/pre-ablation nuclear EKC intensity 15 mpa in ECs of non-  
1127 ablated control ISVs (103 ECs, n=34 larvae), ablated venous ISVs (75 ECs, n=25  
1128 larvae), and ablated arterial ISVs (57 ECs, n=19 larvae). Both venous and arterial  
1129 ISV ECs activate Erk-signalling.

1130 (K) Quantification of post/pre-ablation nuclear EKC intensity 15 mpa in ECs of non-  
1131 ablated uninjected control ISVs (45 ECs, n=15 larvae), non-ablated *spi1/csf3r*  
1132 morphant ISVs (42 ECs, n=14 larvae), uninjected control ISVs (45 ablated/adjacent  
1133 ISV ECs, n=15 larvae), and *spi1/csf3r* morphant ISVs (56 ablated ISV ECs and 57  
1134 adjacent ISV ECs, n=19 larvae). Macrophages are not required to rapidly activate  
1135 Erk-signalling in ablated or adjacent ISV ECs.

1136 (L) Quantification of post/pre-ablation nuclear EKC intensity 15 mpa in ECs of 0.5%  
1137 DMSO-treated non-ablated control ISVs (33 ECs, n=11 larvae), and ISVs of larvae  
1138 treated with either 0.5% DMSO (42 ablated/adjacent ISV ECs, n=14 larvae), 15  $\mu$ M  
1139 SL327 (39 ablated/adjacent ISV ECs, n=13 larvae), 4  $\mu$ M SU5416 (36  
1140 ablated/adjacent ISV ECs, n=12 larvae), 10  $\mu$ M SU5416 (42 ablated/adjacent ISV  
1141 ECs, n=14 larvae), or 500 nM AV951 (42 ablated/adjacent ISV ECs, n=14 larvae).

1142 Vegfr-signalling is not required to rapidly activate Erk-signalling in ablated or  
1143 adjacent ISV ECs.  
1144 ISV: intersegmental vessel. Statistics: Permutation test was conducted for graph H.  
1145 Kruskal Wallis test was conducted for graphs J-L. Error bars represent standard  
1146 deviation. White dotted lines/circle show the wounded sites of each larvae. Scale  
1147 bar: 100  $\mu\text{m}$  for image A, 20  $\mu\text{m}$  for image D.

1148 **Figure 4: Wounded but not adjacent vessels maintain high Erk activity as the**  
1149 **regenerative response proceeds.**

1150 (A-B') Lateral spinning disc confocal images of ablated (A) and adjacent ISVs (B) of  
1151 a 4 dpf EC-EKC larva before and following vessel wounding at indicated timepoints.  
1152 Erk activity is progressively lost in the adjacent but retained in the wounded ISV ECs.  
1153 Images A and B show *fli1aep:EKC* expression, images A' and B' show nuclear  
1154 *fli1aep:EKC* intensity. White dotted lines show the wounded site.

1155 (C,D) Quantification of post/pre-ablation nuclear EKC intensity of ECs in non-ablated  
1156 control ISVs (black, 24 ECs, n=8 larvae), ablated ISVs (red, 30 ECs, n=10 larvae),  
1157 and adjacent ISVs (light blue, 30 ECs, n=10 larvae) before and after vessel  
1158 wounding at indicated timepoints. Graph C shows the quantification of individual ECs  
1159 and graph D shows the average of all biological replicates. At 1 hpa: Control vs  
1160 Ablated ISV ECs:  $p > 0.001$ ; Control vs Adjacent ISV ECs:  $p = 0.108$  (Kruskal Wallis  
1161 test).

1162 ISV: intersegmental vessel. Statistical test: Permutation test was conducted for  
1163 graph C. Error bars represent standard deviation. Scale bar: 20  $\mu\text{m}$

1164

1165 **Figure 5: Erk activity in ablated vessels is maintained through the Vegfr**  
1166 **pathway.**

1167 (A) Ongoing Erk-signalling requires Vegfr and Mek activity. Quantification of  
1168 post/pre-ablation nuclear EKC intensity 3 hpa in ECs of 0.5% DMSO-treated non-  
1169 ablated control ISVs (33 ECs, n=11 larvae), and ablated ISVs of larvae treated with  
1170 either 0.5% DMSO (51 ECs, n=17 larvae), 15  $\mu$ M SL327 (42 ECs, n=14 larvae), 4  
1171  $\mu$ M SU5416 (47 ECs, n=16 larvae), or 10  $\mu$ M SU5416 (32 ECs, n=11 larvae).

1172 (B) *Kdrl* is required for full induction of Erk activity in ablated ISV ECs. Quantification  
1173 of post/pre-ablation nuclear EKC intensity 3 hpa in non-ablated control ISVs ECs of  
1174 uninjected control (27 ECs, n=9 larvae) and *kdrl* crispants (26 ECs, n=9 larvae), and  
1175 ablated ISV ECs of uninjected control (22 ECs, n=8 larvae) and *kdrl* crispants (27  
1176 ECs, n=9 larvae).

1177 (C) Quantification of ISV horizontal length (as percentage of control) for ablated ISVs  
1178 in 24 hpa, 5 dpf, EC-EKC larvae treated with either 0.5% DMSO (n=18 larvae), 4  $\mu$ M  
1179 SU5416 (n=12 larvae), 15  $\mu$ M SL327 (n=15 larvae), or 1  $\mu$ M Trametinib (n=13  
1180 larvae).

1181 (D) Macrophages are not required for maintaining Erk activity in ablated ISV ECs.  
1182 Quantification of post/pre-ablation nuclear EKC intensity 3 hpa in non-ablated control  
1183 ISVs ECs of uninjected control (24 ECs, n=8 larvae) and *spi1/csf3r* morphants (21  
1184 ECs, n=7 larvae), and ablated ISV ECs of uninjected control (29 ECs, n=10 larvae)  
1185 and *spi1/csf3r* morphants (31 ECs, n=11 larvae).

1186 (E-G) Lateral spinning disc confocal images of ablated ISV ECs in 4 dpf 3 hpa EC-  
1187 EKC larvae treated with either 0.5% DMSO (E), 4  $\mu$ M SU5416 (F), or 10  $\mu$ M SU5416  
1188 (G). EC Erk activity was consistently higher and more Vegfr-dependent closer to the  
1189 wound. Arrows indicate first (white), second (yellow), and third (green) ECs from the  
1190 wounded site. Full images: **Figure 5-figure supplementary 1D',H',J'**.

1191 (H) Quantification of post/pre-ablation nuclear EKC intensity at 3 hpa in first (dark  
1192 grey), second (red) and third (light blue) ECs from wound. Treatments were: 0.5%  
1193 DMSO-treated non-ablated control ISVs (11 first, second and third ECs, n=11  
1194 larvae), and ablated ISVs of larvae treated with either 0.5% DMSO (17 first, second  
1195 and third ECs, n=17 larvae), 4  $\mu$ M SU5416 (16 first and second ECs, and 15 third  
1196 ECs, n=16 larvae), or 10  $\mu$ M SU5416 (11 first and second ECs, and 10 third ECs,  
1197 n=11 larvae). The same embryos were used in A.

1198 (I) Quantification of post/pre-ablation nuclear EKC intensity at 3 hpa in first (14 ECs,  
1199 n=14 larvae), second (14 ECs, n=14 larvae), third (14 ECs, n=14 larvae), fourth (11  
1200 ECs, n=11 larvae), and fifth (8 ECs, n=8 larvae) ECs from the wounded site of  
1201 ablated ISVs in 4 dpf EC-EKC larvae. Data for the first, second, and third ECs were  
1202 taken from **Figure 4-figure supplement 1N**.

1203 ISV: intersegmental vessel. DA: dorsal aorta. Statistical test: Kruskal Wallis test was  
1204 conducted for graphs A,C,D,H,I. ordinary one-way ANOVA test was conducted for  
1205 graph B. Error bars represent standard deviation. 15  $\mu\text{m}$  for image E.

1206



1207 **Figure 6: Ca<sup>2+</sup> signalling is required for rapid Erk activation in ablated vessels.**

1208 (A) Still images from **Video 8** demonstrating a pulse of Ca<sup>2+</sup> signalling immediately  
1209 adjacent to the wound (4 dpf). Left panels show *actb2:GCaMP6f* and *kdrl:mCherry-*  
1210 *CAAX*, right panels show *actb2:GCaMP6f*. Yellow arrows show ISV ECs with active  
1211 Ca<sup>2+</sup> signalling. Blue arrows show Ca<sup>2+</sup> signalling in recruited immune cells.

1212 (B) Quantification of *actb2:GCaMP6f* intensity in unablated control ISVs (black, n=4  
1213 larvae), ablated (red, n=10 larvae) and adjacent (light blue, n =10 larvae) ISVs  
1214 following wounding. Intensity was normalised to *actb2:GCaMP6f* intensity in  
1215 unablated tissue in the same larvae.

1216 (C) Ca<sup>2+</sup> signalling is required for rapid activation of Erk signalling in ablated ISV  
1217 ECs. Quantification of post/pre-ablation nuclear EKC intensity at 15 mpa in ECs of  
1218 1% DMSO-treated non-ablated control ISVs (39 ECs, n=13 larvae), and ISVs of  
1219 larvae treated with either 1% DMSO (39 ablated/adjacent ISV ECs, n=13 larvae) or  
1220 50 µM Nifedipine (36 ablated/adjacent ISV ECs, n=12 larvae).

1221 (D) Quantification of post/pre-ablation nuclear EKC intensity at 15 mpa in ECs of 1%  
1222 DMSO-treated non-ablated control ISVs (18 ECs, n=6 larvae), and ISVs of larvae  
1223 treated with either 1% DMSO (27 ablated/adjacent ISV ECs, n=9 larvae) or 100 µM  
1224 Amplopidine (31 ablated ISV ECs and 33 adjacent ISV ECs, n=11 larvae).

1225 (E) Ca<sup>2+</sup> signalling is not required for sustaining Erk activity in ablated ISV ECs.  
1226 Quantification of post/pre-ablation nuclear EKC intensity at 3 hpa in ECs of 1%  
1227 DMSO-treated non-ablated control ISVs (24 ECs, n=8 larvae), and ablated ISVs of  
1228 larvae treated with either 1% DMSO (42 ECs, n=14 larvae) or 50 µM Nifedipine (39  
1229 ECs, n=13 larvae) for 30 minutes before 3 hpa (**Figure 6-figure supplement 2A**).

1230 (F) Quantification of post/pre-ablation nuclear EKC intensity at 3 hpa in ECs of 1%  
1231 DMSO-treated non-ablated control ISVs (21 ECs, n=7 larvae), and ablated ISVs of  
1232 larvae treated with either 1% DMSO (27 ECs, n=9 larvae) or 50 µM Nifedipine (27  
1233 ECs, n=9 larvae) for 30 minutes after vessel wounding (**Figure 6-figure supplement**  
1234 **2H**).

1235 (G,G') Still images from **Video 3** showing ablated ISV ECs of a 4 dpf EC-EKC larva  
1236 at after vessel wounding. Activation of Erk progresses from the wound to the vessel  
1237 base. Image G show the *fli1aep:EKC* expression, G' shows nuclear *fli1aep:EKC*  
1238 intensity. Arrows indicate first (white), second (yellow), third (green), forth (red), and  
1239 fifth (orange) ECs from the wounded site.

1240 (H) Quantification of nuclear EKC intensity (normalised to nuclear EKC intensity at 2  
1241 mpa) in ECs of ISVs in non-ablated control larvae (black, 24 ECs, n=8 larvae), and  
1242 the first (red, 9 ECs, n=9 larvae), second (blue, 9 ECs, n=9 larvae), third (green, 9  
1243 ECs, n=9 larvae), fourth (orange, 8 ECs, n=8 larvae), and fifth (purple, 5 ECs, n=5  
1244 larvae) ablated ISV ECs from the wounded site following vessel wounding.  
1245 ISV: intersegmental vessel. Statistical test: Kruskal Wallis test was conducted for  
1246 graphs C-F. two-sample Kolmogorov-Smirnov test was conducted for graph H. Error  
1247 bars represent standard deviation. Scale bars: 50  $\mu\text{m}$  for image A, 15  $\mu\text{m}$  for image  
1248 G.

1249 **Figure 7: A two-step mechanism for activating and maintaining Erk activity in**  
1250 **regenerating vessels.**

1251 Schematic representation of the two-step mechanism employed by ECs to activate  
1252 Erk-signalling following vessel wounding. Pre-ablation (left), the majority of ECs are  
1253 Erk-signalling inactive. Following vessel wounding (middle), both ablated and  
1254 adjacent ISV ECs rapidly activate Erk-signalling. Ca<sup>2+</sup> signalling is also rapidly  
1255 activated following vessel wounding but only in ablated ISV ECs, particularly in ECs  
1256 close to the wounded site. Ca<sup>2+</sup> signalling activity contributes to the activation of Erk-  
1257 signalling in ablated ISV ECs in a sequential manner, starting from ECs close to the  
1258 wounded site. Erk-signalling in adjacent ISV ECs has returned to pre-wound levels  
1259 by 3 hpa (right). Erk activity in ablated vessel ISV ECs is sustained through Vegfr-  
1260 signalling. ECs closer to the wounded site are less sensitive to Vegfr-signalling  
1261 inhibition, with higher signalling compared to ECs further away. Recruited  
1262 macrophages are essential for vessel regeneration but not the sole source of Vegfs  
1263 at 3 hpa.

1264

1265

1266 **Supplementary figures and figure legends**

1267

1268 **Figure 1 - figure supplement 1: The EC-EKC transgenic line reports tip cell**  
1269 **enriched and cell-state dependent Erk-signalling during primary angiogenesis.**

1270 (A-A'') Lateral spinning disc confocal images of budding ISVs in a 22 hpf EC-EKC  
1271 embryo show high Erk activity in ISV tip ECs. Image A shows the *fli1aep:EKC*  
1272 expression, image A' shows both the *fli1aep:EKC* and the *fli1a:H2B-mCherry*  
1273 expression, while image A'' shows the nuclear *fli1aep:EKC* expression intensity.  
1274 Yellow arrows point to DA ECs with nuclear depleted EKC localisation.

1275 (B) Quantification of the nucleus/cytoplasm EKC intensity ratio in sprouting ISV tip  
1276 ECs of 22 hpf embryos (0.803, 133 ECs, n=37 embryos) showing consistently higher  
1277 levels in cytoplasm.

1278 (C) Quantification of the sprouting ISV tip EC/DA stalk EC nuclear EKC intensity ratio  
1279 with two different methods in 22 hpf embryos (109 ECs, n=37 embryos). DA ECs  
1280 closest to the sprouting ISV ECs were quantified. Ratios were calculated using a  
1281 value of nuclear EKC/H2B-mCherry intensity in tip cells (0.777) or using a raw  
1282 nuclear EKC intensity measurement alone in tip cells (0.817), both showed higher  
1283 Erk activity in sprouting ISV tip ECs when compared to DA stalk ECs.

1284 (D-E'') Nuclear ellipticity and Erk-activity correlate. Lateral spinning disc confocal  
1285 images of either an ISV with "migrating EC" (D) or an ISV with "non-migrating EC"  
1286 (E) in 28 hpf EC-EKC embryos. Migrating or non-migrating determined by position  
1287 relative to the DLLV. D and E; *fli1aep:EKC* expression, D' and E'; *fli1aep:EKC* and  
1288 *fli1a:H2B-mCherry*, D'' and E''; nuclear *fli1aep:EKC* expression intensity. Light blue  
1289 arrow shows ISV stalk ECs with nuclear depleted EKC localisation.

1290 (F) Quantification of EC ellipticity in "migrating" (125 ECs, n=45 embryos) and "non-  
1291 migrating" ISV leading ECs based on position relative to DLLV (63 ECs, n=35  
1292 embryos) at 28 hpf.

1293 (G) More migratory ECs, with more elliptical nuclei, show higher Erk activity.  
1294 Quantification of tip/stalk ISV EC nuclear EKC intensity for the most elliptic (47 ECs,  
1295 n=30 embryos) or less elliptical (oblate) nuclei (47 ECs, n=29 embryos) in 28 hpf  
1296 embryos. Most elliptic (upper quartile of all migrating ECs in F) and oblate (lower  
1297 quartile of all non-migrating ECs in F) nuclei were quantified.

1298 ISV: intersegmental vessel; DA: dorsal aorta. Statistical test: Mann-Whitney test was  
1299 conducted for graphs C, F and G. Error bars represent standard deviation. Scale  
1300 bars: 25  $\mu\text{m}$  for image A, 15  $\mu\text{m}$  for image D.

1301 **Figure 3 - figure supplement 1: Rapid Erk activation is largely restricted to**  
1302 **wounded and adjacent ISV ECs.**

1303 (A-B') Lateral confocal images of 4 dpf EC-EKC larvae pre-ablation (A,A') and 15  
1304 mpa (B,B'). Immediately adjacent ISV ECs show rapid Erk activation, while Erk  
1305 activity in 2<sup>nd</sup> and 3<sup>rd</sup> adjacent ISV ECs are largely unchanged. White dotted line  
1306 shows the wounded site.

1307 (C) Quantification of post/pre-ablation nuclear EKC intensity at 15 mpa in ECs of  
1308 non-ablated control ISVs (30 ECs, n=10 larvae), and adjacent (27 ECs, n=9 larvae),  
1309 2<sup>nd</sup> adjacent (27 ECs, n=9 larvae), and 3<sup>rd</sup> adjacent ISVs (27 ECs, n=9 larvae).

1310 DA, dorsal aorta; ISV: intersegmental vessel. Statistical test: Kruskal Wallis test was  
1311 conducted for graph C. Error bars represent standard deviation. Scale bar: 50  $\mu$ m for  
1312 image A.

1313

1314

1315

1316

1317 **Figure 3 - figure supplement 2: Macrophages are not required for rapid Erk**  
1318 **activation following vessel wounding.**

1319 (A-C) Lateral spinning disc confocal images of 4 dpf  
1320 *Tg(kdrl:EGFP);Tg(mpeg1:mCherry)* larvae pre-ablation (A), 15 mpa (B), or 3 hpa (C).

1321 Macrophages are recruited to the wounded site by 3 hpa but not by 15 mpa.

1322 (D) Quantification of macrophage number recruited to the wounded site pre-ablation  
1323 (n=25 embryos), 15 mpa (n=14 embryos) or 3 hpa (n=24 embryos).

1324 (E,F) Lateral spinning disc confocal images of 3 dpf *Tg(mpeg1:mCherry)* uninjected  
1325 control (E) or *spi1/csf3r* morphants (F).

1326 (G) Quantification of macrophage number within the trunk spanning 3 somites length  
1327 in 3 dpf *Tg(mpeg1:mCherry)* uninjected control (n=29 embryos) or *spi1/csf3r*  
1328 morphants (n=25 embryos).

1329 (H,I) Macrophages are required for vessel regeneration. Lateral confocal images of  
1330 24 hpa, 4 dpf, *Tg(fli1aep:EKC)* uninjected control (H) or *spi1/csf3r* morphants (I).

1331 (J) Quantification of ISV horizontal length (as percentage of control) for ablated ISVs  
1332 in 24 hpa, 4 dpf, EC-EKC uninfected control (n=11 larvae) or *spi1/csf3r* morphants  
1333 (n=13 larvae).

1334 (K-V') Lateral spinning disc confocal images of ISV ECs in 3 dpf EC-EKC uninjected  
1335 control (K-L', O-P', S-T') and *spi/csf3r* morphants (M-N', Q-R', U-V'). Erk-signalling is  
1336 rapidly activated in both ablated and adjacent ISV ECs in larvae with reduced  
1337 macrophage number. Images K-N' show non ablated control ISV ECs, images O-R'  
1338 show ablated ISV ECs, images S-V' show adjacent ISV ECs. Images O,Q,S,U were  
1339 taken pre-ablation, images P,R,T,V were taken 15 mpa. Images K-V show the  
1340 *fli1aep:EKC* expression, and images K'-V' shows the nuclear *fli1aep:EKC* intensity.

1341 ISV: intersegmental vessel; Statistical test: Kruskal Wallis test was conducted for  
1342 graph D and Mann-Whitney test was conducted for graph G and J. Error bars  
1343 represent standard deviation. White dotted lines/circles show the wounded sites of  
1344 each embryos/larvae. Scale bars: 20  $\mu$ m for image A, 50  $\mu$ m for image E and H, 15  
1345  $\mu$ m for image K.

1346

1347 **Figure 3 - figure supplement 3: Vegfr-signalling is not required for rapid Erk**  
1348 **activation following vessel wounding.**

1349 **(A-B'')** Lateral spinning disc confocal images of ISV ECs in 28 hpf EC-EKC embryos  
1350 treated for an hour with either 0.5% DMSO (A-A''), with active EC Erk-signalling; or  
1351 500 nM AV951 (B-B''), with inactive EC Erk-signalling. Images A and B show the  
1352 *fli1aep:EKC* expression, while images A' and B' show both the *fli1aep:EKC* and the  
1353 *fli1a:H2B-mCherry* expression. Images A'' and B'' show the nuclear *fli1aep:EKC*  
1354 intensity.

1355 **(C)** Quantification of nucleus/cytoplasm EKC intensity in ISV tip ECs of 28 hpf  
1356 embryos treated with either 0.5% DMSO (0.849, 65 ECs, n=14 embryos) or 500 nM  
1357 AV951 (1.423, 53 ECs, n=12 embryos).

1358 **(D-Z')** Vegfr-signalling inhibitors do not block rapid Erk-signalling activation in  
1359 ablated and adjacent ISVs following vessel wounding. Lateral spinning disc confocal  
1360 images of ISV ECs in 4 dpf EC-EKC larvae treated with either 0.5% DMSO (D-I'), 15  
1361  $\mu$ M SL327 (J-M'), 4  $\mu$ M SU5416 (O-R'), 10  $\mu$ M SU5416 (S-V'), or 500 nM AV951 (W-  
1362 Z'). Images D-E' show non-ablated control ISV ECs. Images F-G', J-K', O-P', S-T'  
1363 and W-X' show ablated ISV ECs. Images H-I', L-M', Q-R', U-V' and Y-Z' show  
1364 adjacent ISV ECs. Images F,H,J,L,O,Q,S,U,W,Y were taken pre-ablation and images  
1365 G,I,K,M,P,R,T,V,X,Z were taken 15 mpa. Images D-Z show the *fli1aep:EKC*  
1366 expression, and images D'-Z' show the nuclear *fli1aep:EKC* intensity. White dotted  
1367 lines show the wounded sites of each larvae.

1368 ISV: intersegmental vessel; Statistical test: Mann-Whitney test was conducted for  
1369 graph C. Error bars represent standard deviation. Scale bars: 25  $\mu$ m for image A, 15  
1370  $\mu$ m for image D.

1371



1372 **Figure 4 - figure supplement 1: Distinct Erk activity between ablated and**  
1373 **adjacent ISV ECs 3 hpa.**

1374 (A-I') Lateral spinning disc confocal images of ISV ECs in 4 dpf EC-EKC larvae at  
1375 indicated timepoints. Images A-I show the *fli1aep:EKC* expression, while images A'-I'  
1376 show the nuclear *fli1aep:EKC* intensity.

1377 (J-M') Erk signalling is activated in ablated, but not adjacent ISV ECs at 3 hpa.  
1378 Lateral spinning disc confocal images of ablated and adjacent ISV ECs in 4 dpf EC-  
1379 EKC larvae before (J-K'), and 3 hours following vessel wounding (L-M'). Images J-M  
1380 show the *fli1aep:EKC* expression, while images J'-M' show the nuclear *fli1aep:EKC*  
1381 intensity. Images K and M are higher magnification images of the yellow boxes in  
1382 images J and L. White circle in image L shows the wounded site. Arrows indicate  
1383 first (white), second (yellow), third (green), fourth (red), and fifth (orange) ECs from  
1384 the wounded site.

1385 (N) Quantification of post/pre-ablation nuclear EKC intensity of ECs in non-ablated  
1386 control ISVs (27 ECs, n=9 larvae), ablated ISVs (42 ECs, n=14 larvae), and adjacent  
1387 ISVs (42 ECs, n=14 larvae) 3 hpa.

1388 ISV: intersegmental vessel; Statistical test: Kruskal Wallis test was conducted for  
1389 graph N. Error bars represent standard deviation. Scale bars: 20  $\mu\text{m}$  for image A, 20  
1390  $\mu\text{m}$  for images J and K.

1391

1392 **Figure 4 - figure supplement 2: Vessel wounding is required for sustained Erk**  
1393 **activity in ablated ISV ECs.**

1394 (A,B) Vessels that are not wounded do not sustain Erk activity. Lateral spinning disc  
1395 confocal images of ISV ECs in 4 dpf EC-EKC larvae at 0 min/pre-ablation (left), 15  
1396 minutes/15 mpa (middle), or 3 hours/3 hpa (right). Images A show ISVs in non-  
1397 ablated control larvae, and images B show ISVs in larvae with tissue ablated in  
1398 between two ISVs (Control ablation). Images A and B show the *fli1aep:EKC*  
1399 expression, while images A' and B' show the nuclear *fli1aep:EKC* intensity. White  
1400 dotted lines show the wounded site.

1401 (C) Quantification of post/pre-ablation nuclear EKC intensity of ECs in either non-  
1402 ablated control ISVs or control ablation ISVs at 15 mpa (control, 39 ECs, n=13  
1403 larvae; control ablation, 48 ECs, n=16 larvae) or 3 hpa (control, 18 ECs, n=6 larvae;  
1404 control ablation, 24 ECs, n=8 larvae).

1405 ISV: intersegmental vessel; Statistical test: Kruskal Wallis test was conducted for  
1406 graph C. Error bars represent standard deviation. Scale bar: 15  $\mu$ m

1407 **Figure 5 - figure supplement 1: Vegfr-signalling is required to sustain Erk**  
1408 **activity in ablated ISV ECs following vessel wounding.**

1409 (A-J') Lateral spinning disc confocal images of ISV ECs in 4 dpf EC-EKC larvae  
1410 treated with either 0.5% DMSO (A-D'), 15  $\mu$ M SL327 (E-F'), 4  $\mu$ M SU5416 (G-H'), or  
1411 10  $\mu$ M SU5416 (I-J'). A higher concentration of SU5416 (10  $\mu$ M) is required to block  
1412 the Erk activity in ablated ISV ECs 3 hpa immediately adjacent to the wound. Images  
1413 A-B' show non-ablated control ISV ECs. Images C,E,G,I were taken pre-ablation and  
1414 images D,F,H,J were taken 3 hpa. Images A-J show the *fli1aep:EKC* expression,  
1415 and images A'-J' show the nuclear *fli1aep:EKC* intensity.

1416 (K,L) Lateral confocal images of 4 dpf EC-EKC uninjected control (n=100/100) (K)  
1417 and *kdrl* crispant (n=98/103 larvae displayed phenotype indicated) (L). *kdrl* crispants  
1418 phenocopy previously published *kdrl* mutant/morphant vascular phenotypes.

1419 (M-T') High Erk activity is not maintained in *kdrl* crispants 3 hpa. Lateral confocal  
1420 images of ISV ECs in 4 dpf EC-EKC uninjected control (M-N', Q-R') and *kdrl*  
1421 crispants (O-P', S-T'). Images M-P' show non ablated control ISV ECs, images Q-T'  
1422 show ablated ISV ECs. Images Q and S were taken pre-ablation, images R and T  
1423 were taken 3 hpa. Images M-T show the *fli1aep:EKC* expression, and images M'-T'  
1424 show the nuclear *fli1aep:EKC* intensity.

1425 (U-X) Erk-signalling is required for vessel regeneration. Lateral spinning disc  
1426 confocal images of 24 hpa 5 dpf EC-EKC larvae treated with either: 0.5% DMSO (U),  
1427 showing a regenerated ISV; or 4  $\mu$ M SU5416 (V), 15  $\mu$ M SL327 (W), or 1  $\mu$ M  
1428 Trametinib (X); all of which blocked ISV regeneration.

1429 DA, dorsal aorta; ISV: intersegmental vessel. White dotted lines/circles show the  
1430 wounded site of each larvae. Scale bars: 15  $\mu$ m for image A, 100  $\mu$ m for image K, 20  
1431  $\mu$ m for image A, 50  $\mu$ m for image U.

1432

1433 **Figure 5 - figure supplement 2: Macrophages are not required to sustain Erk**  
1434 **activity in ablated ISV ECs following vessel wounding.**

1435 (A-H') Lateral confocal images of ISV ECs in 3 dpf EC-EKC uninjected control (A-B',  
1436 E-F') and *spi1/csrf3r* morphants (C-D', G-H'). Images A-D' show non-ablated control  
1437 ISV ECs. Images E and G were taken pre-ablation and images F and H were taken 3  
1438 hpa. Images A-H show the *fli1aep:EKC* expression, and images A'-H' show the  
1439 nuclear *fli1aep:EKC* intensity. White dotted lines show the wounded site of each  
1440 embryo.

1441 ISV: intersegmental vessel. Scale bar: 20  $\mu$ m.

1442

1443

1444

1445

1446

1447 **Figure 6 - figure supplement 1: Ca<sup>2+</sup> signalling is required for rapid Erk**  
1448 **activation in ablated ISV ECs.**

1449 (A-T') Ca<sup>2+</sup> signalling is required for rapid Erk activation. Lateral spinning disc  
1450 confocal images of ISV ECs in 4 dpf EC-EKC larvae treated with either 1% DMSO  
1451 (A-D',G-H',K-N',Q-R'), 50 μM Nifedipine (E-F',I-J'), or 100 μM Amlodipine (O-P',S-  
1452 T'). Images A-B' and K-L' show non-ablated control ISV ECs. Images  
1453 C,E,G,I,M,O,Q,S were taken pre-ablation and images D,F,H,J,N,P,R,T were taken  
1454 15 mpa. Images A-T show the *fli1aep:EKC* expression, and images A-T' show the  
1455 nuclear *fli1aep:EKC* intensity. White dotted lines show the wounded site of each  
1456 larvae.

1457 ISV: intersegmental vessel. Scale bar: 15 μm

1458 **Figure 6 - figure supplement 2: Ca<sup>2+</sup> signalling is not required for sustained Erk**  
1459 **activation in ablated ISV ECs.**

1460 (A) Schematic representation of imaging schedule for larvae in images B-G.

1461 (B-G') Ca<sup>2+</sup> signalling is required not required for sustaining Erk activation in ablated  
1462 ISV ECs. Lateral spinning disc confocal images of ISV ECs in 4 dpf EC-EKC larvae  
1463 treated with either 1% DMSO (A-E') or 50 μM Nifedipine (F-G'). Images B-C' show  
1464 non-ablated control ISV ECs. Images D and F were taken pre-ablation and images E  
1465 and G were taken 3 hpa. Images B-G show the *fli1aep:EKC* expression, and images  
1466 B-G' show the nuclear *fli1aep:EKC* intensity.

1467 (H) Schematic representation of imaging schedule for larvae in images I-N.

1468 (I-N') Lateral confocal images of ISV ECs in 4 dpf EC-EKC larvae treated with either  
1469 1% DMSO (I-L') or 50 μM Nifedipine (M-N'). Images I-J' show non-ablated control  
1470 ISV ECs. Images K and M were taken pre-ablation and images L and N were taken 3  
1471 hpa. Images I-N show the *fli1aep:EKC* expression, and images I-N' show the nuclear  
1472 *fli1aep:EKC* intensity.

1473 ISV: intersegmental vessel. White dotted lines show the wounded site of each  
1474 larvae.

1475 Scale bar: 15 μm

1476

1477

1478 **Videos**

1479

1480 **Video 1: ISV daughter ECs show asymmetric Erk activity following cytokinesis.**

1481 Time-lapse video of an ISV tip EC undergoing mitosis in a 24-25 hpf EC-EKC  
1482 embryo. Left panel shows the *fli1aep:EKC* expression, middle panel shows the  
1483 *fli1a:H2B-mCherry* expression, and the right panel shows the nuclear *fli1aep:EKC*  
1484 intensity. Z stacks were acquired every 15.5 seconds for 40 minutes using an Andor  
1485 Dragonfly Spinning Disc Confocal microscope. Photobleaching was minimised using  
1486 the bleach correction tool (correction method: Histogram Matching) in FIJI.

1487 ISV: intersegmental vessel; DA: dorsal aorta. Scale bar: 25  $\mu\text{m}$ .

1488

1489 **Video 2: ISV ECs in 4 dpf larvae have minimal Erk activity.**

1490 Time-lapse video of the trunk vessels in a 4 dpf EC-EKC larva at indicated  
1491 timepoints. ECs in functional vessels at 4 dpf have low Erk activity. Left panel shows  
1492 the *fli1aep:EKC* expression, middle panel shows both *fli1aep:EKC* and *fli1a:H2B-*  
1493 *mCherry* expression, and the right panel shows the nuclear *fli1aep:EKC* intensity. Z  
1494 stacks were acquired every minute for 41 minutes using an Andor Dragonfly  
1495 Spinning Disc Confocal microscope. Photobleaching was minimised using the bleach  
1496 correction tool (correction method: Histogram Matching) in FIJI.

1497 ISV: intersegmental vessel; DA: dorsal aorta. Scale bar: 20  $\mu\text{m}$ .

1498



1499 **Video 3: Both ablated and adjacent ISV ECs rapidly activate Erk-signalling**  
1500 **following vessel wounding.**

1501 Time-lapse video of the trunk vessels in a 4 dpf EC-EKC larva before (pre-ablation)  
1502 and after (post-ablation) vessel wounding at indicated timepoints. Vessel wounding  
1503 rapidly activates Erk-signalling in both ablated and adjacent ISV ECs. Post-ablation  
1504 video starts at 2 minutes post-ablation due to the time taken to transfer the larvae  
1505 between microscopes and for preparation of imaging. Left panel shows the  
1506 *fli1aep:EKC* expression, middle panel shows both *fli1aep:EKC* and *fli1a:H2B-*  
1507 *mCherry* expression, and the right panel shows the nuclear *fli1aep:EKC* intensity. Z  
1508 stacks were acquired every 1 minute for 20 minutes before and after vessel  
1509 wounding using an Andor Dragonfly Spinning Disc Confocal microscope.  
1510 Photobleaching was minimised using the bleach correction tool (correction method:  
1511 Histogram Matching) in FIJI.

1512 ISV: intersegmental vessel; DA: dorsal aorta. Scale bar: 20  $\mu\text{m}$ .

1513

1514

1515 **Video 4: Ablated ISV ECs rapidly activate Erk-signalling following vessel**  
1516 **wounding.**

1517 Time-lapse video of the ablated ISV in a 4 dpf EC-EKC larva before (pre-ablation)  
1518 and after (post-ablation) vessel wounding at indicated timepoints. Post-ablation video  
1519 starts at 2 minutes post-ablation due to the time taken to transfer the larvae between  
1520 microscopes and for preparation of imaging. Left panel shows the *fli1aep:EKC*  
1521 expression and the right panel shows the nuclear *fli1aep:EKC* intensity. Z stacks  
1522 were acquired every 1 minute for 20 minutes before and after vessel wounding using  
1523 an Andor Dragonfly Spinning Disc Confocal microscope. Photobleaching was  
1524 minimised using the bleach correction tool (correction method: Histogram Matching)  
1525 in FIJI.

1526 ISV: intersegmental vessel. Scale bar: 20  $\mu\text{m}$ .

1527

1528 **Video 5: Adjacent ISV ECs rapidly activate Erk-signalling following vessel**  
1529 **wounding.**

1530 Time-lapse video of the adjacent ISV in a 4 dpf EC-EKC larva before (pre-ablation)  
1531 and after (post-ablation) vessel wounding at indicated timepoints. Post-ablation video  
1532 starts at 2 minutes post-ablation due to the time taken to transfer the larvae between  
1533 microscopes and for preparation of imaging. Left panel shows the *fli1aep:EKC*  
1534 expression and the right panel shows the nuclear *fli1aep:EKC* intensity. Z stacks  
1535 were acquired every 1 minute for 20 minutes before and after vessel wounding using  
1536 an Andor Dragonfly Spinning Disc Confocal microscope. Photobleaching was  
1537 minimised using the bleach correction tool (correction method: Histogram Matching)  
1538 in FIJI.

1539 ISV: intersegmental vessel. Scale bar: 20  $\mu\text{m}$ .

1540

1541

1542 **Video 6: Skin epithelial and muscle cells do not maintain high Erk activity for 3**  
1543 **hours following muscle wounding.**

1544 Time-lapse video of the trunk in a 30 hpf *Tg(ubb:Mmu.Elk1-KTR-mCherry)* embryo  
1545 following muscle wounding. The white circle shows the wounded site. Skin epithelial  
1546 and muscle cells surrounding the wounded site do not sustain Erk activity (examples  
1547 of Erk active cells, with nuclear excluded EKC expression indicated with white  
1548 arrows). Z stacks were acquired every 21 minutes from 5 mpa until 3 hpa using a  
1549 Leica SP8 X WLL confocal microscope (n=6 embryos).

1550 Scale bar: 20  $\mu$ m.

1551

1552 **Video 7: ISVs in 4 dpf larvae do not have active Ca<sup>2+</sup> signalling.**  
1553 Time-lapse video of ISVs in a 4 dpf *Tg(actb2:GCaMP6f);Tg(kdr:mCherry-CAAX)*  
1554 larva. Functional vessels at 4 dpf have low or undetectable Ca<sup>2+</sup> signalling. Left  
1555 panel shows both the *actb2:GCaMP6f* and the *kdr:mCherry-CAAX* expression and  
1556 the right panel shows the *actb2:GCaMP6f* expression. Z stacks were acquired every  
1557 minute for 15 minutes using a Leica SP8 confocal microscope.  
1558 ISV: intersegmental vessel. Scale bar: 50 μm.  
1559

1560 **Video 8: ISVs rapidly activate Ca<sup>2+</sup> signalling following vessel wounding.**  
1561 Time-lapse video of both ablated and adjacent ISVs in a 4 dpf  
1562 *Tg(actb2:GCaMP6f);Tg(kdrl:mCherry-CAAX)* larva following vessel wounding. Only  
1563 the wounded ISV activates Ca<sup>2+</sup> signalling. Left panel shows both the  
1564 *actb2:GCaMP6f* and the *kdrl:mCherry-CAAX* expression and the right panel shows  
1565 the *actb2:GCaMP6f* expression. Z stacks were acquired every minute from 5 mpa  
1566 until 20 mpa using a Leica SP8 confocal microscope.  
1567 ISV: intersegmental vessel. Scale bar: 50 μm.  
1568

1569 **Figure source data**

1570

1571 **Figure 1-source data 1: Nuclear/cytoplasm EKC measurements in leading ISV**  
1572 **ECs of DMSO, SL327, and SU5416-treated 28 hpf embryos.**

1573

1574 **Figure 1-figure supplement 1-source data 1: EKC measurements in ISV ECs at**  
1575 **22 and 28 hpf.**

1576

1577 **Figure 2-source data 1: Tip/stalk nuclear EKC measurements in ISV ECs**  
1578 **following cell division.**

1579

1580 **Figure 3-source data 1: Post/pre-ablation nuclear EKC measurements in**  
1581 **control, ablated, and adjacent ISV ECs.**

1582

1583 **Figure 3-figure supplement 1-source data 1: Post/pre-ablation nuclear EKC**  
1584 **measurements in adjacent, 2<sup>nd</sup> adjacent and 3<sup>rd</sup> adjacent ISV ECs 15 mpa**

1585

1586 **Figure 3-figure supplement 2-source data 1: Measurements of macrophage**  
1587 **number and ISV length.**

1588

1589 **Figure 3-figure supplement 3-source data 1: Nuclear/cytoplasm EKC**  
1590 **measurements in leading ISV ECs of DMSO and AV951-treated 28 hpf**  
1591 **embryos.**

1592

1593 **Figure 4-source data 1: Post/pre-ablation nuclear EKC measurements in**  
1594 **control, ablated, and adjacent ISV ECs from pre-ablation to 3 hpa.**

1595

1596 **Figure 4-figure supplement 1-source data 1: Post/pre-ablation nuclear EKC**  
1597 **measurements in control, ablated, and adjacent ISV ECs at 3 hpa.**

1598

1599 **Figure 4-figure supplement 1-source data 1: Post/pre-ablation nuclear EKC**  
1600 **measurements in control and control ablated ISV ECs at 15 mpa and 3 hpa.**

1601

1602 **Figure 5-source data 1: Post/pre-ablation nuclear EKC measurements in**  
1603 **control, ablated, and adjacent ISV ECs at 3 hpa.**

1604 **Figure 6-source data 1: GCaMP6f intensity measurements and post/pre-**  
1605 **ablation nuclear EKC measurements in control, ablated, and adjacent ISV ECs.**

1606

1607



**Figure 1**

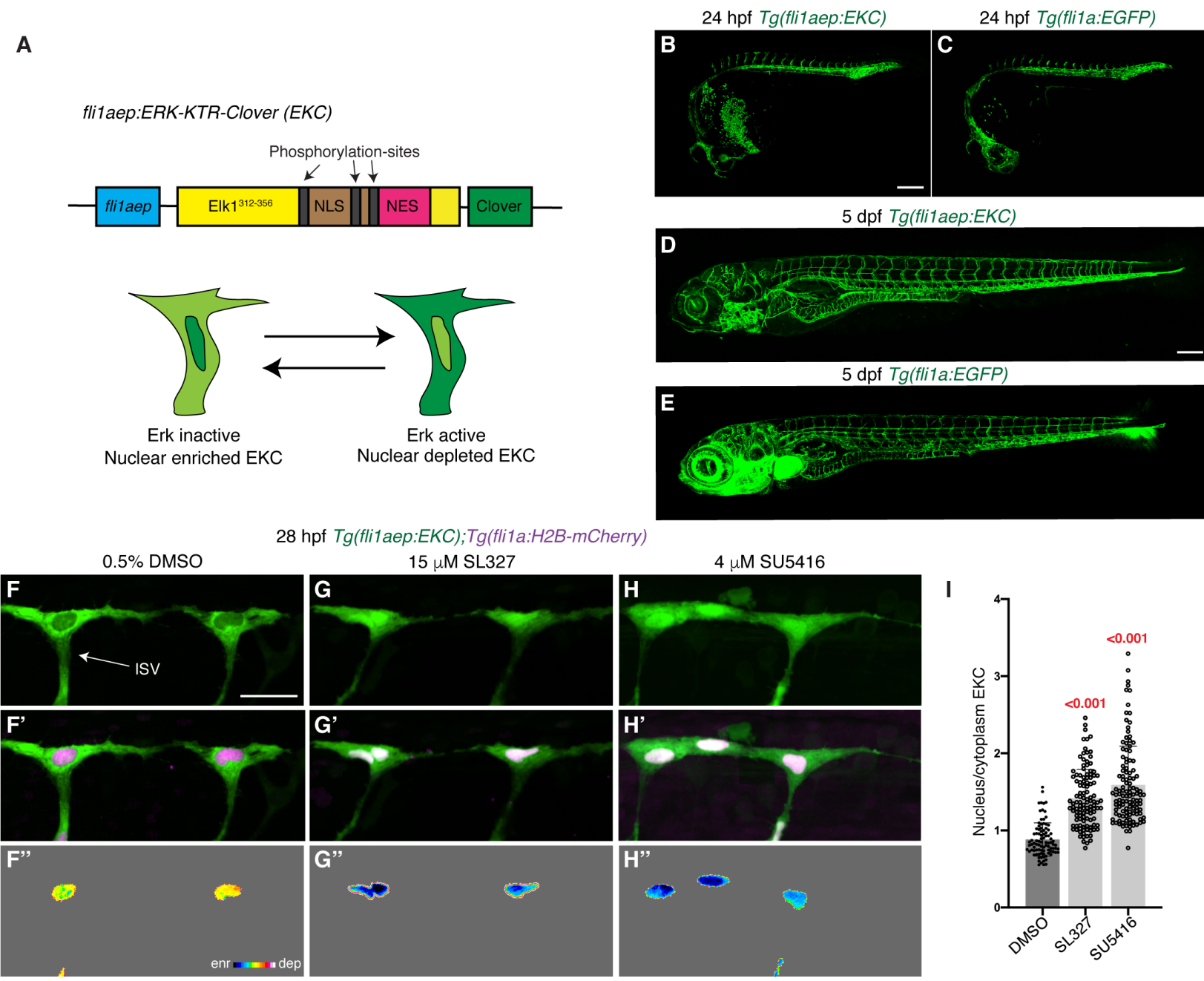
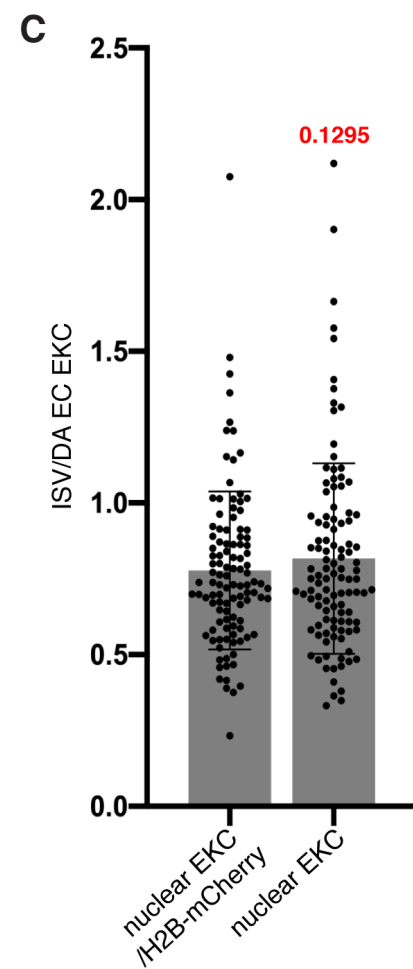
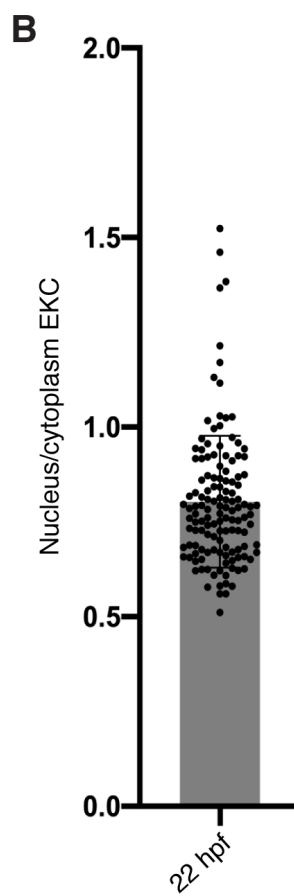
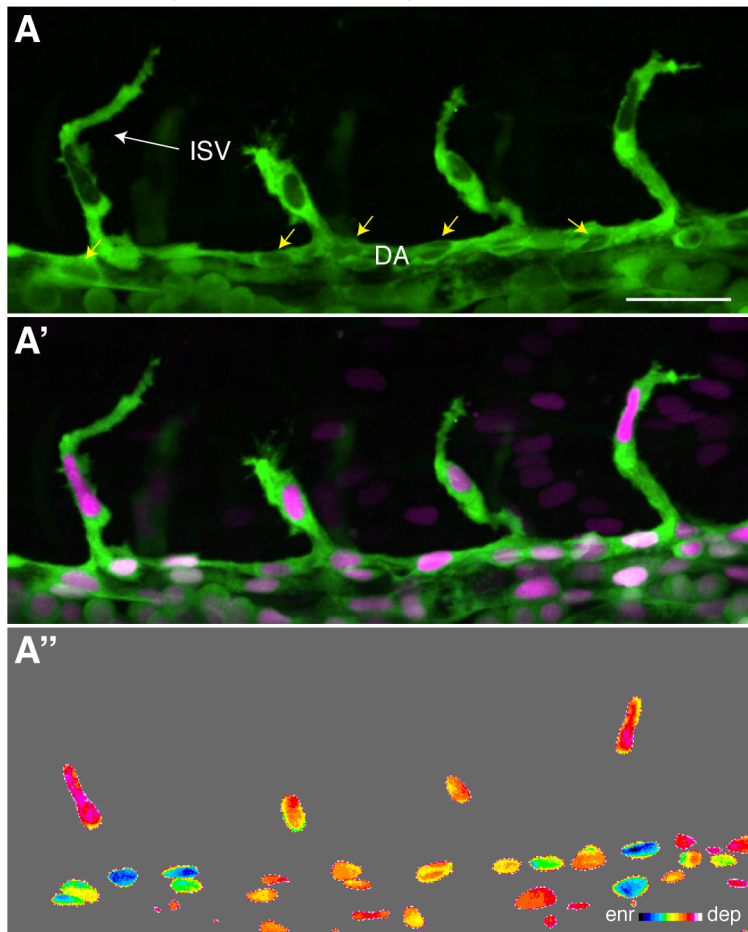


Figure 1-figure supplement 1

22 hpf *Tg(fli1aep:EKC);Tg(fli1a:H2B-mCherry)*



28 hpf *Tg(fli1aep:EKC);Tg(fli1a:H2B-mCherry)*

Migrating EC Non-migrating EC

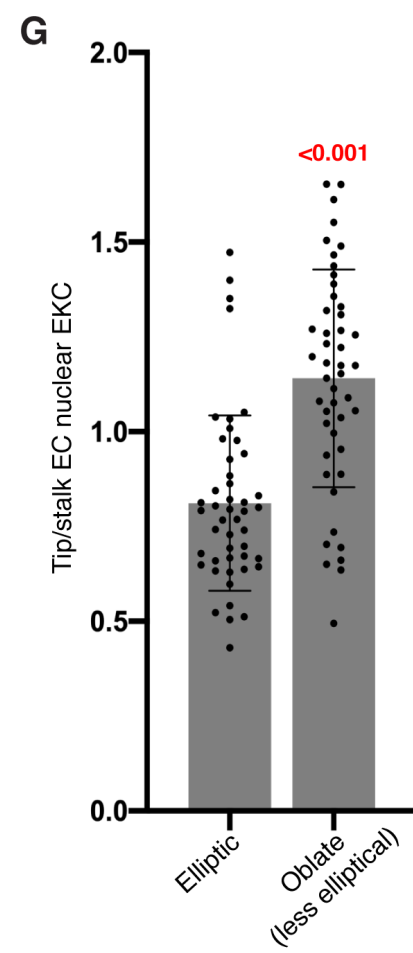
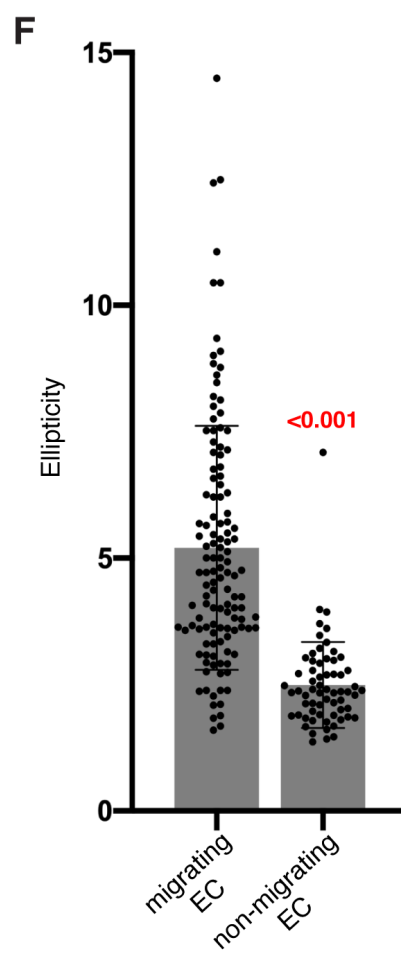
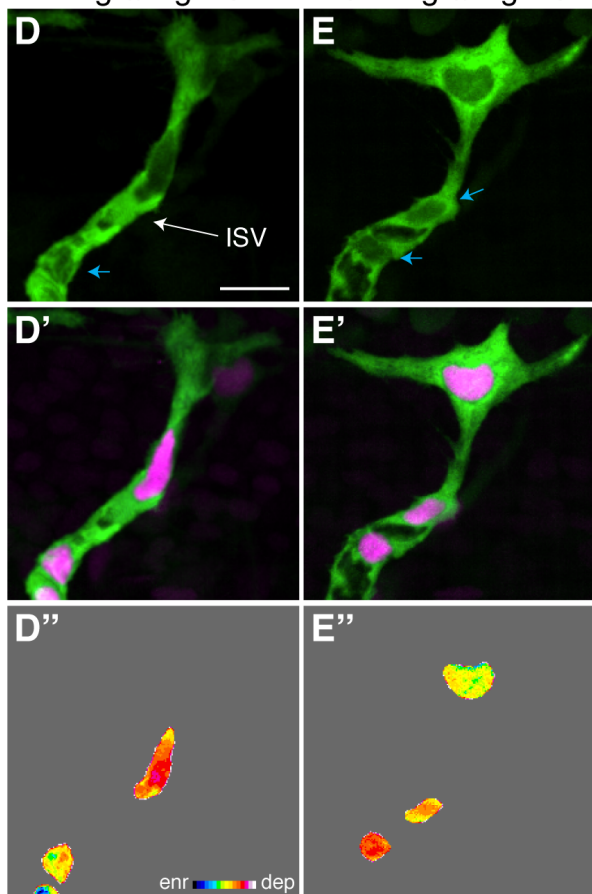


**Figure 2**

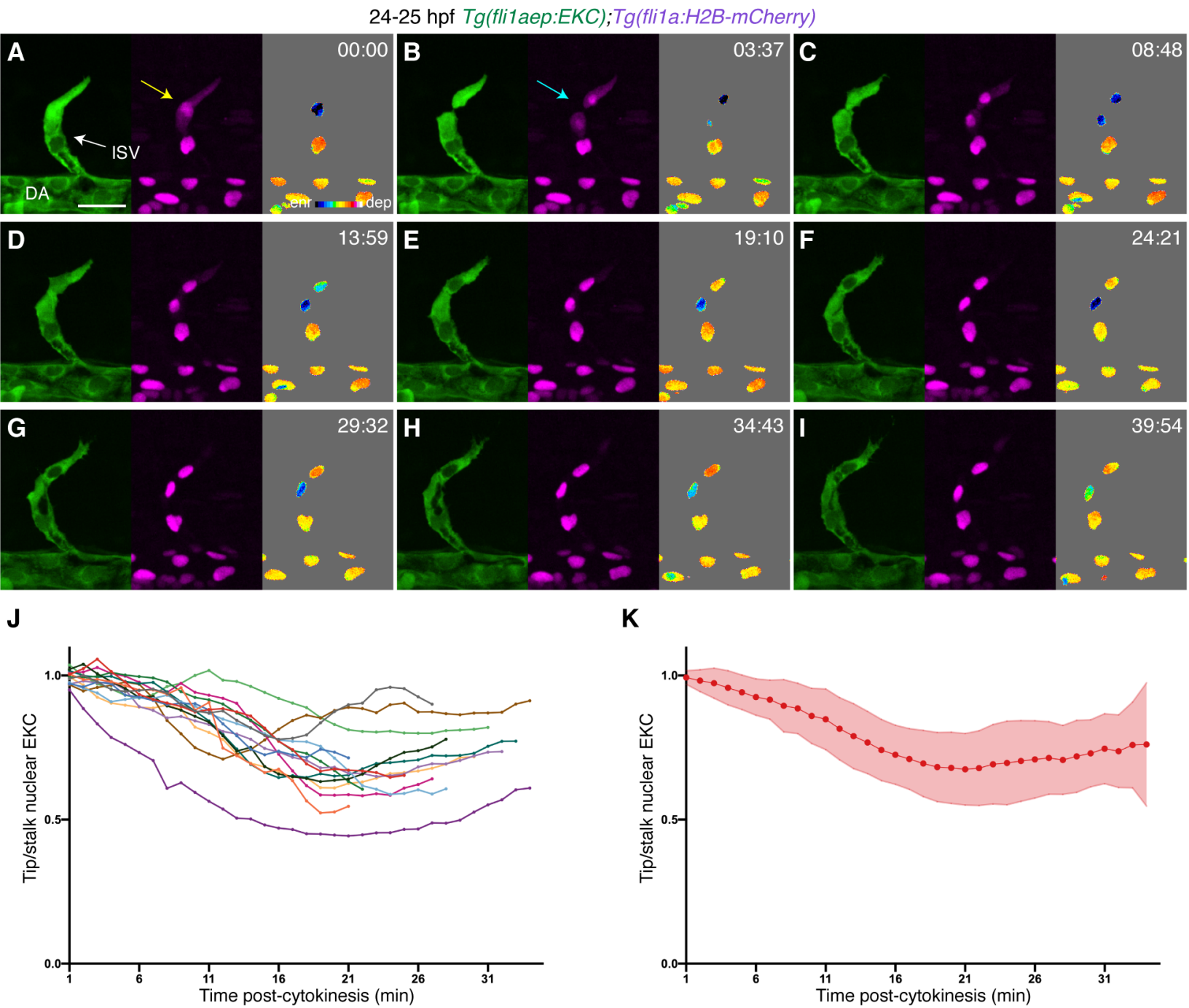






# Figure 3-figure supplement 1

4 dpf *Tg(fli1aep:EKC);Tg(fli1a:H2B-mCherry)*  
 Pre-ablation 15 mpa

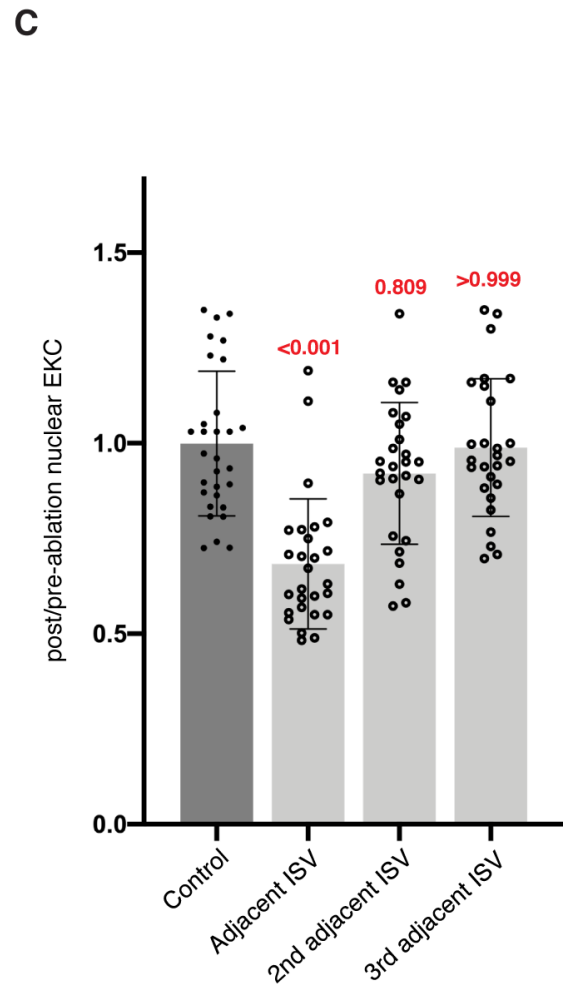
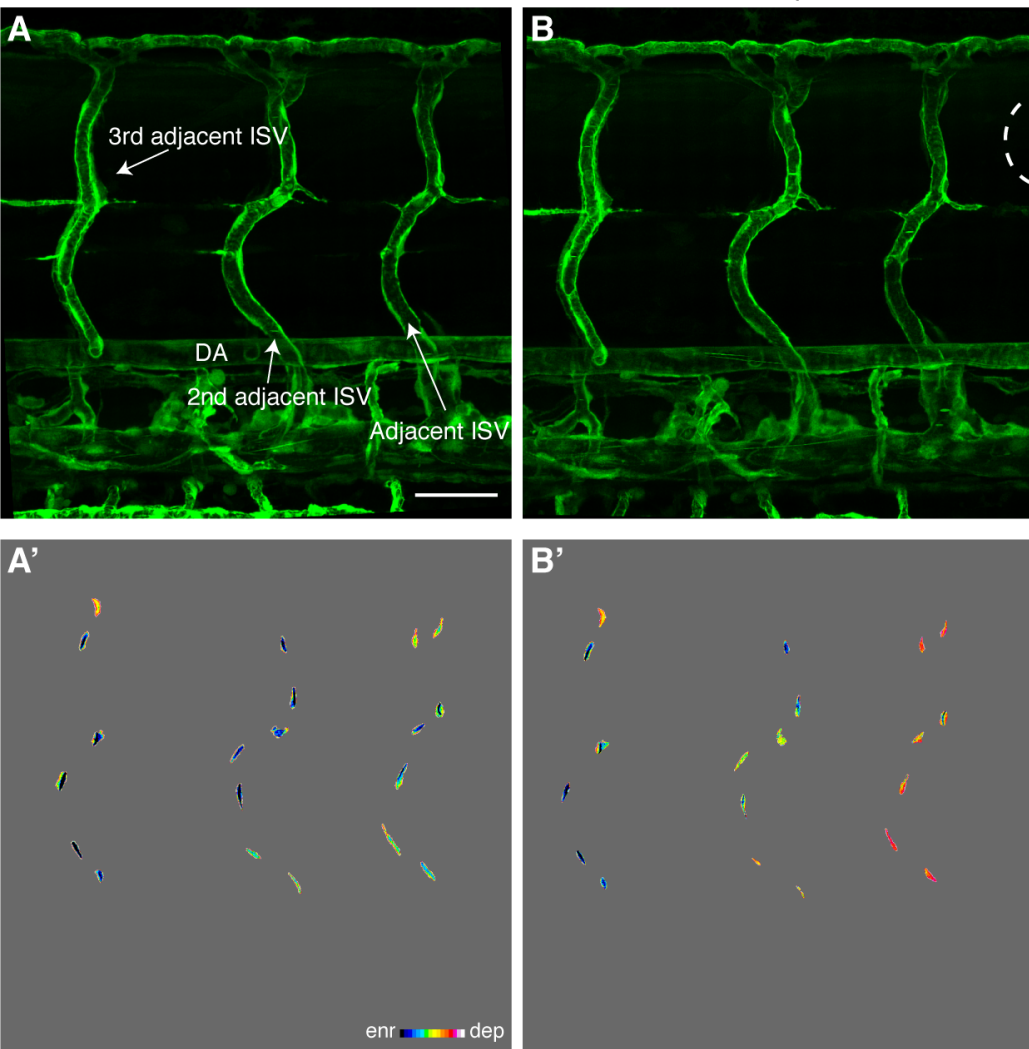


# Figure 3-figure supplement 2

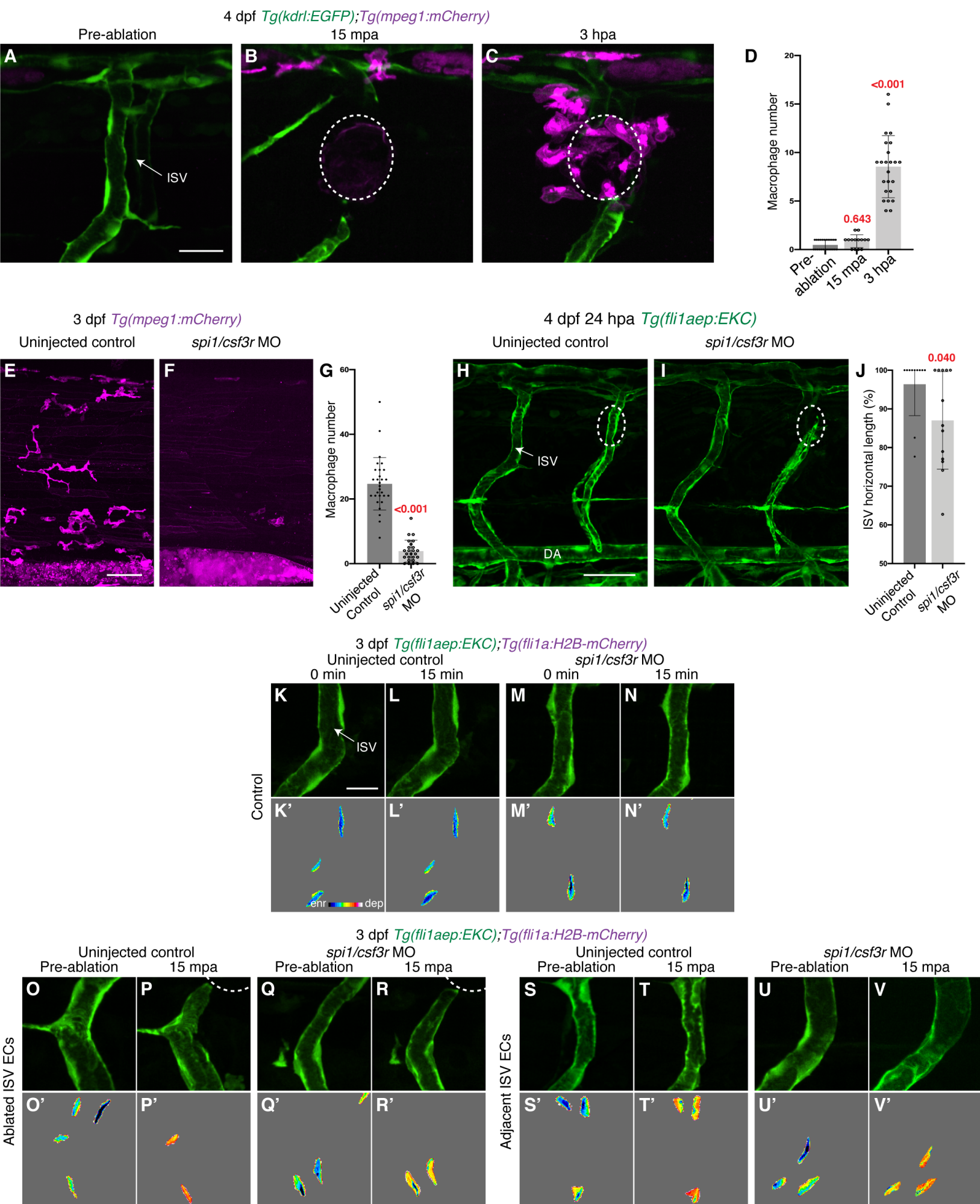




**Figure 3-figure supplement 3**

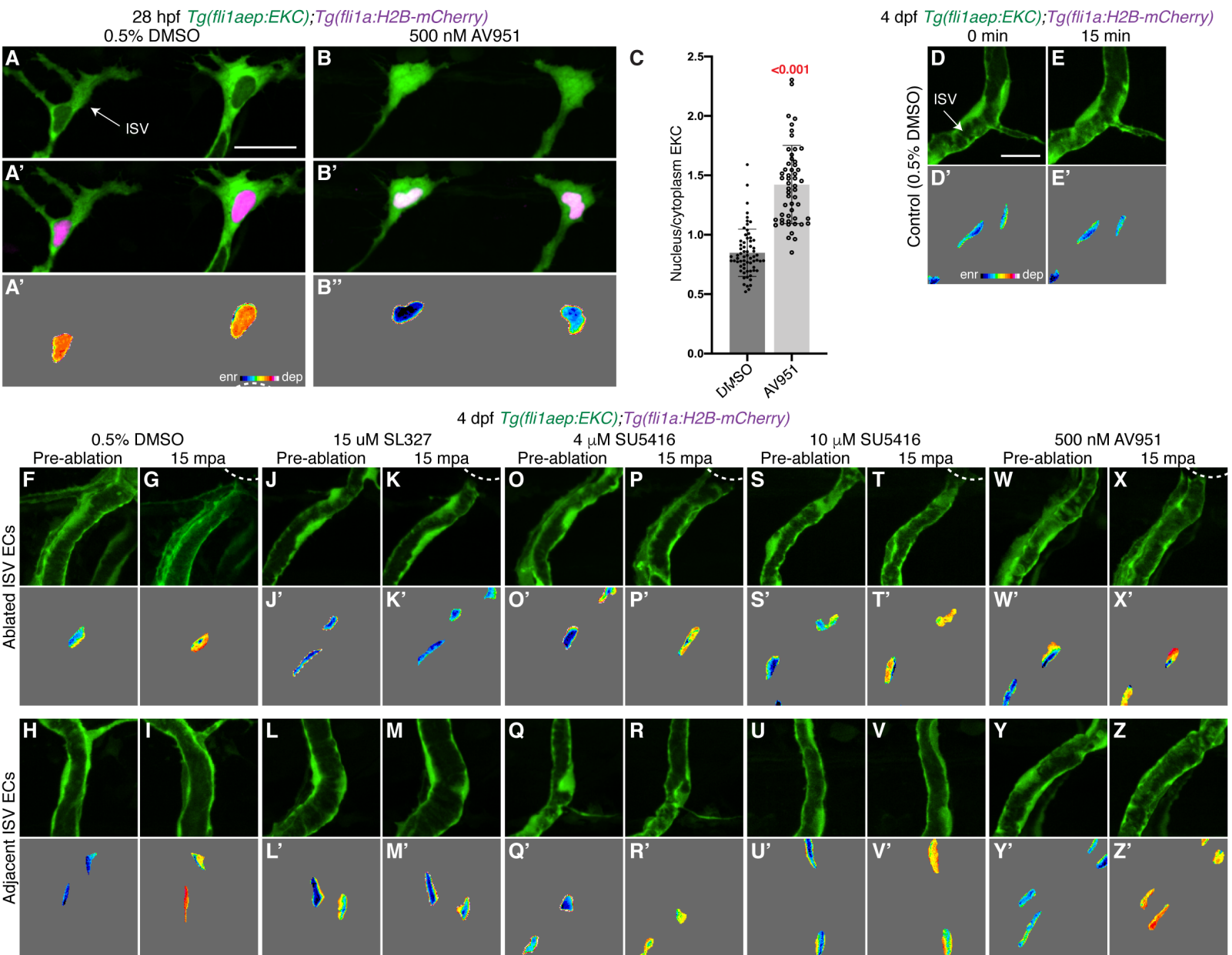


**Figure 4**

4 dpf *Tg(fli1aep:EKC);Tg(fli1a:H2B-mCherry)*

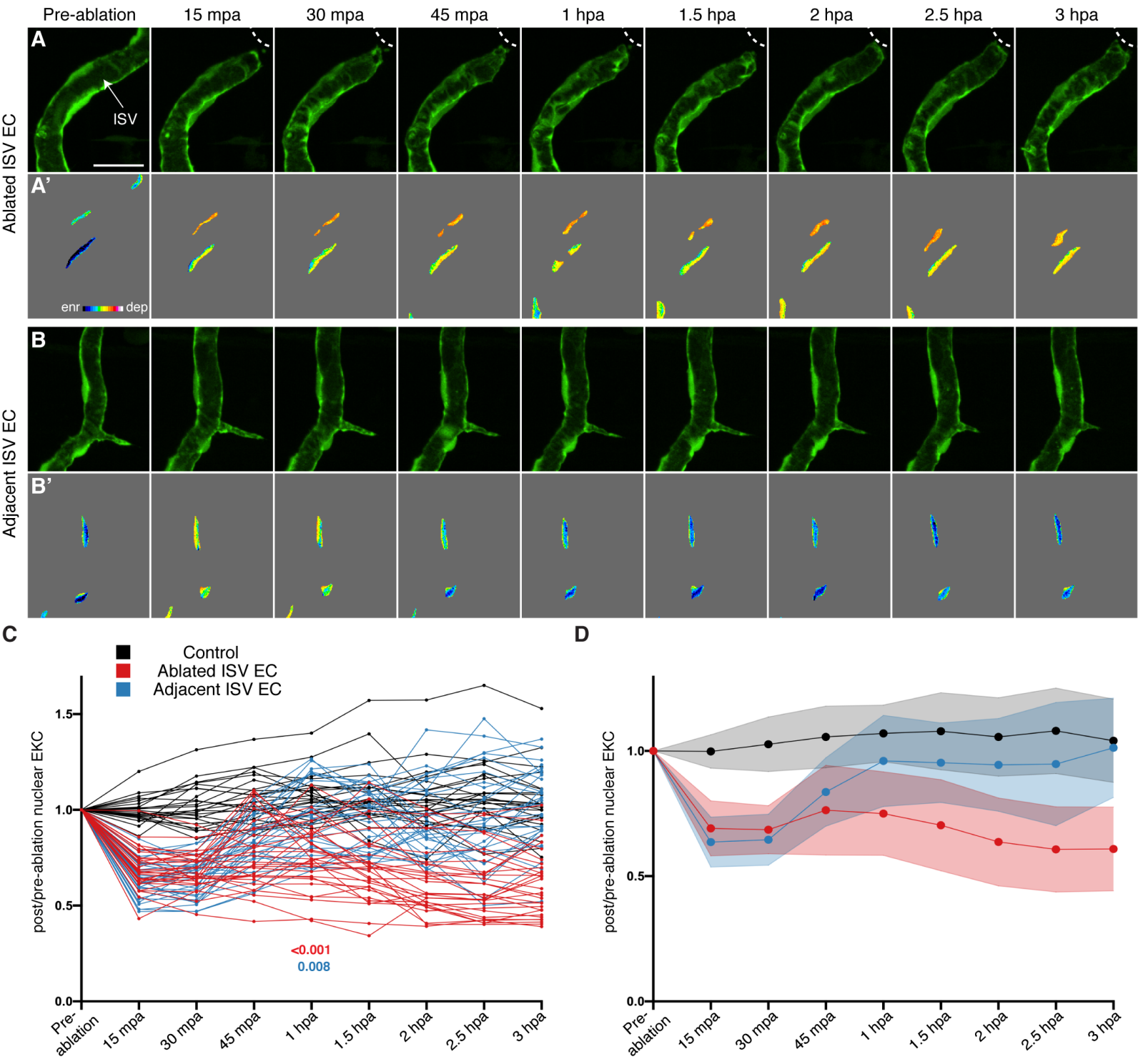






**Figure 4-figure supplement 2**

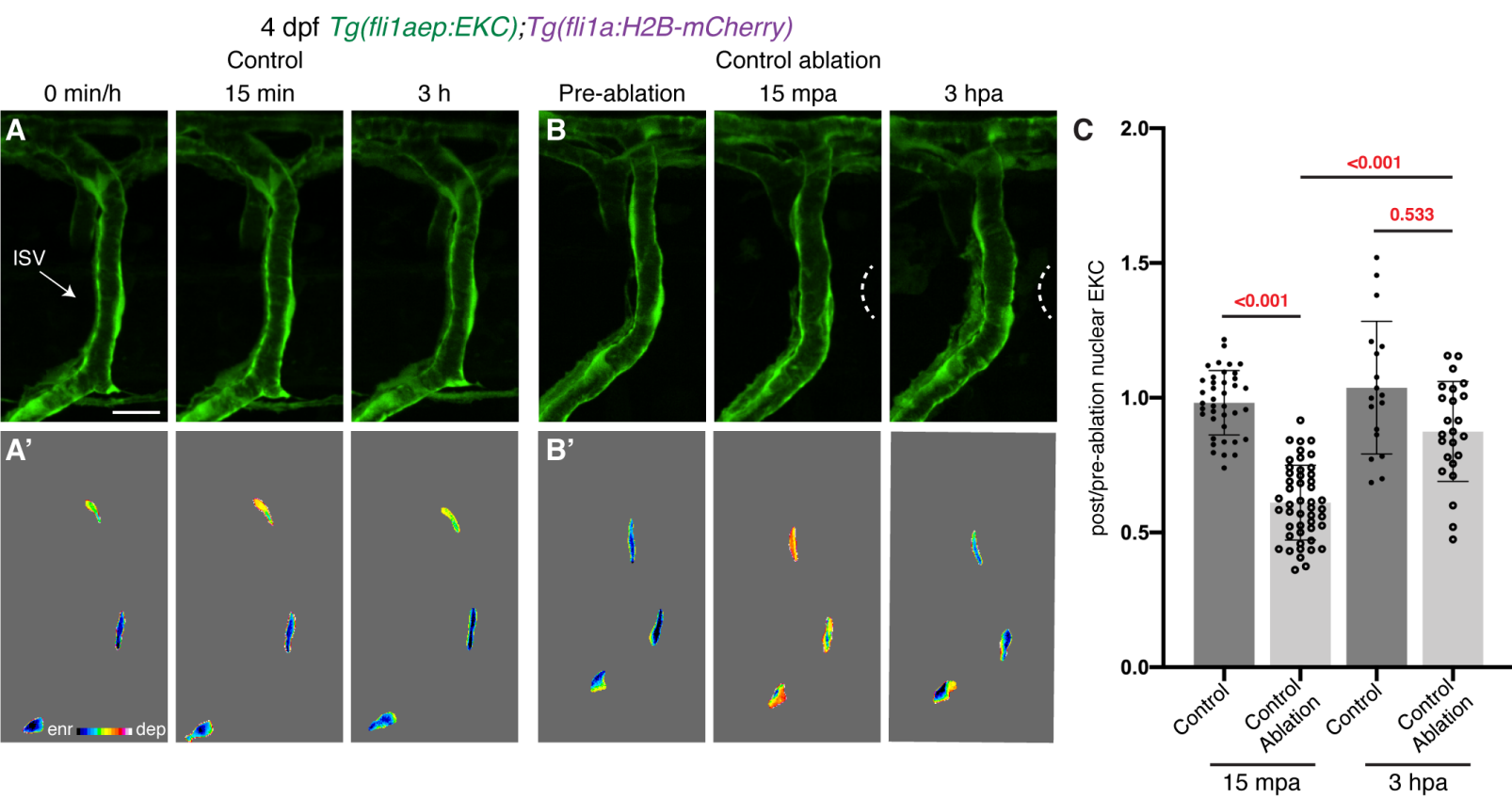


**Figure 5**

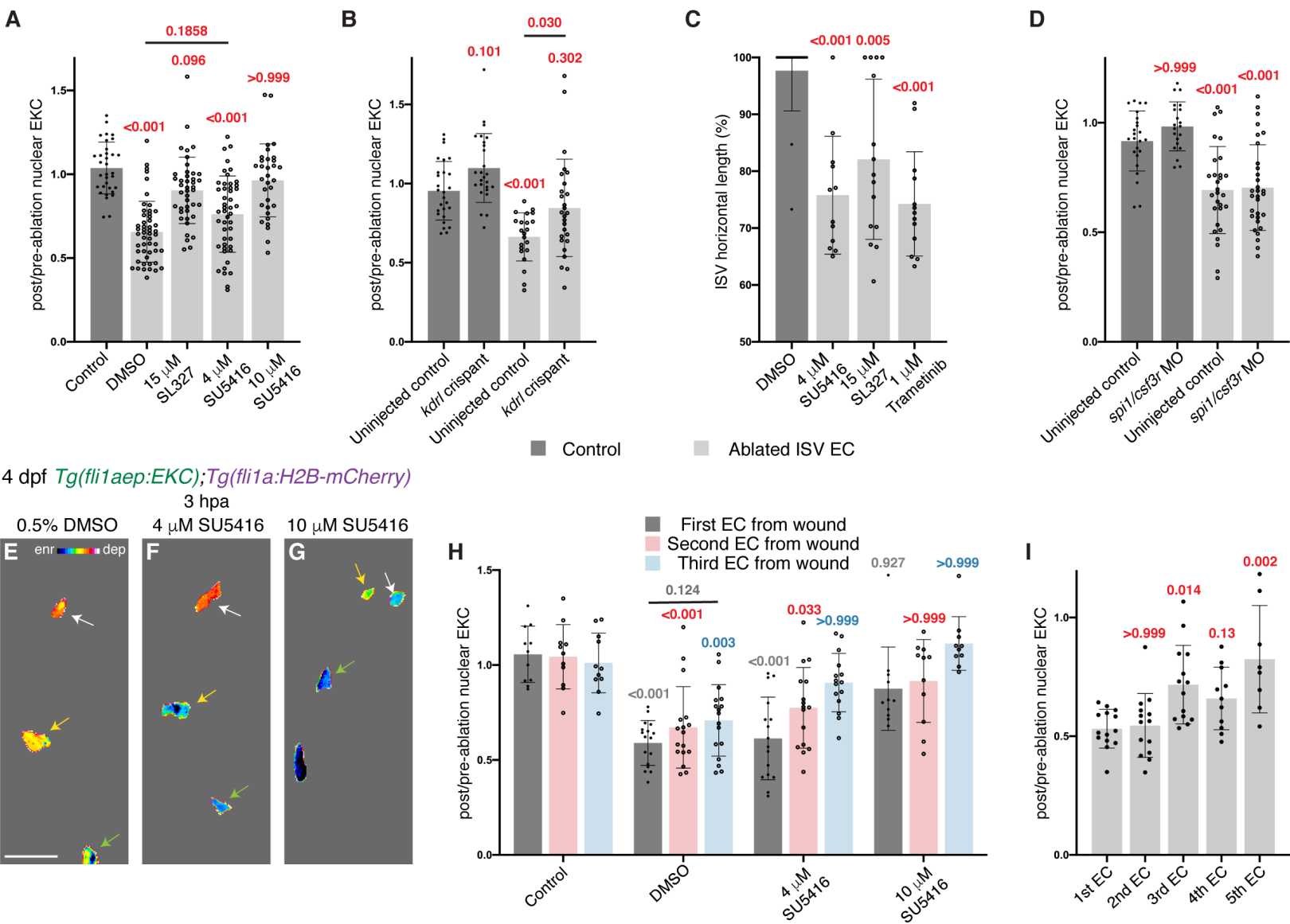


# Figure 5-figure supplement 1

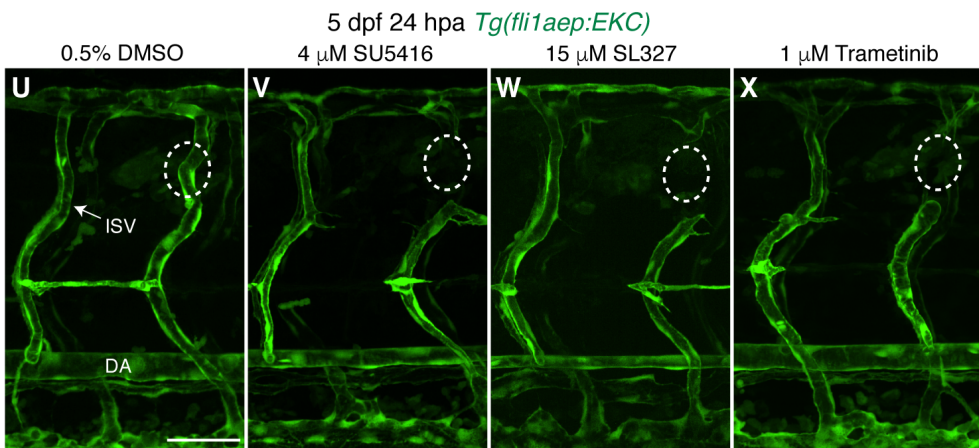
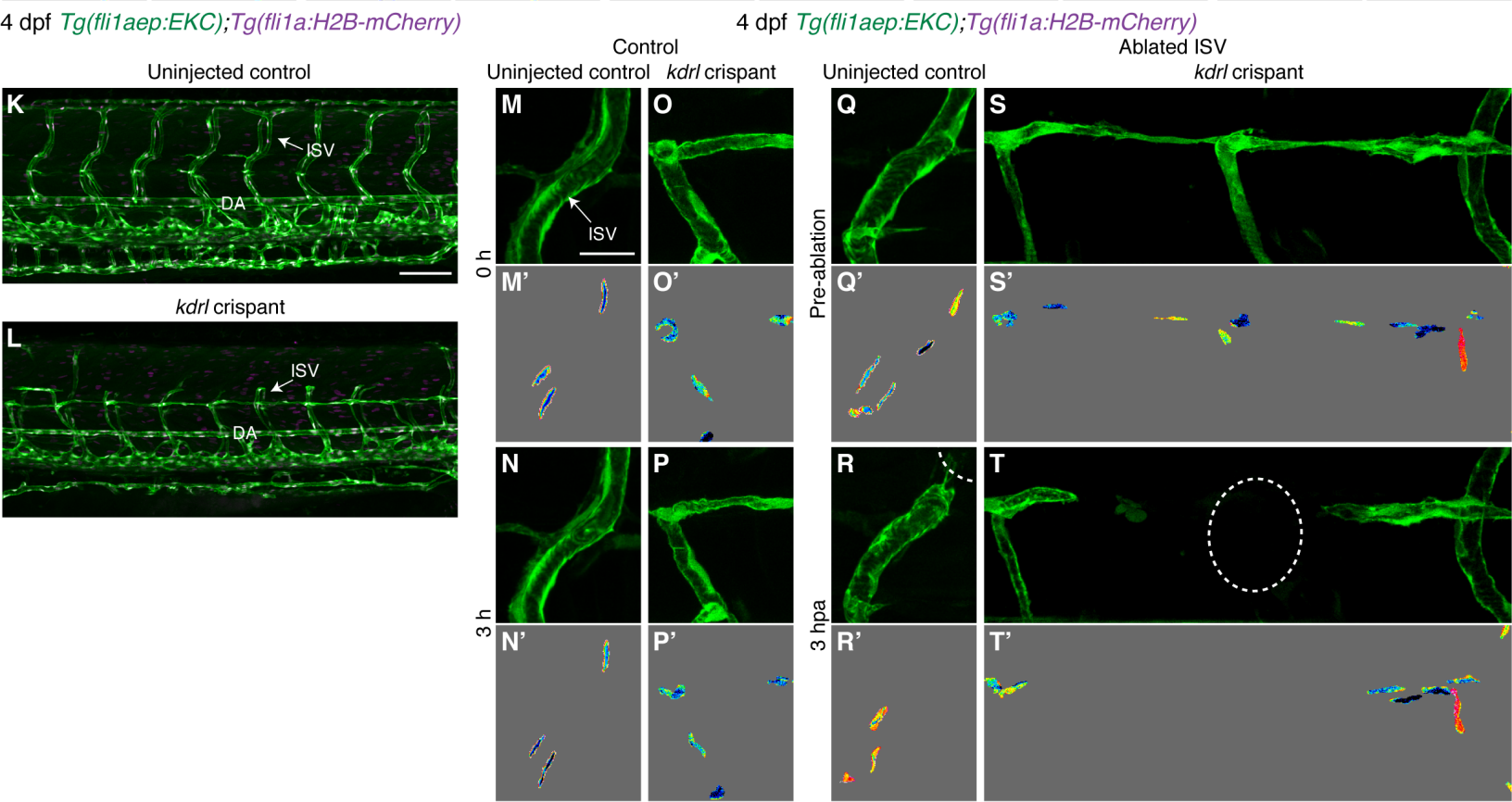
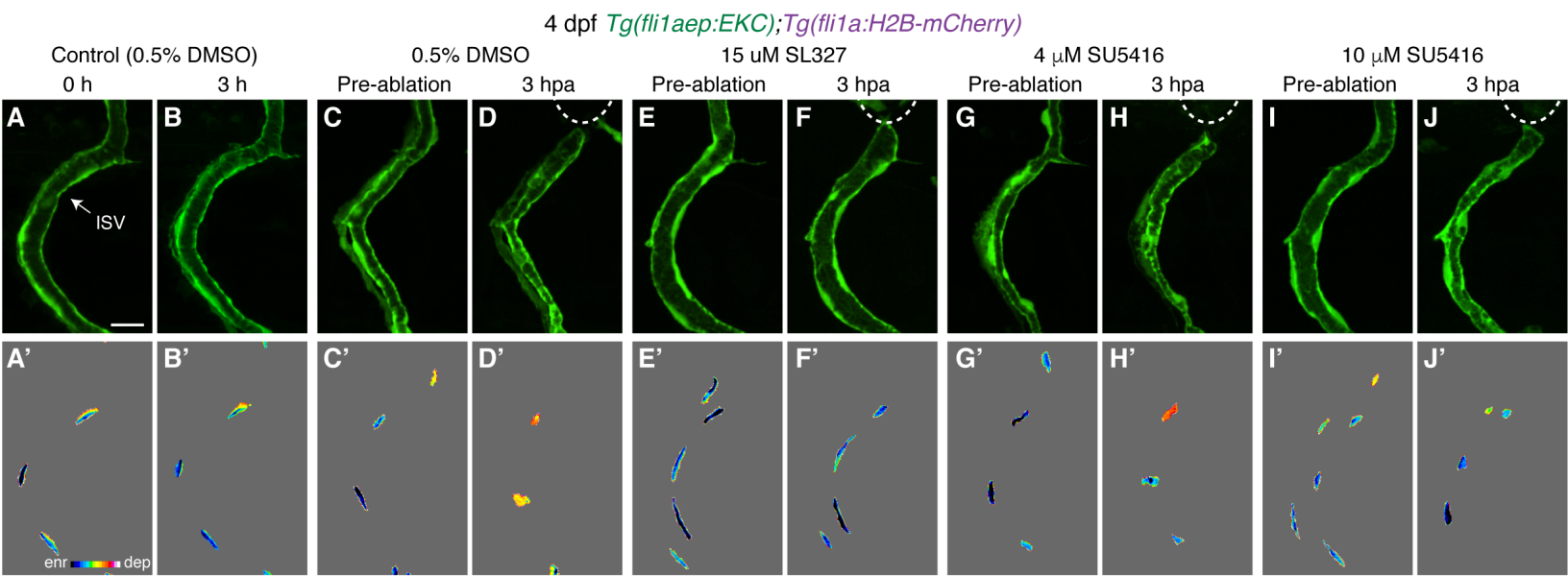


**Figure 5-figure supplement 2**

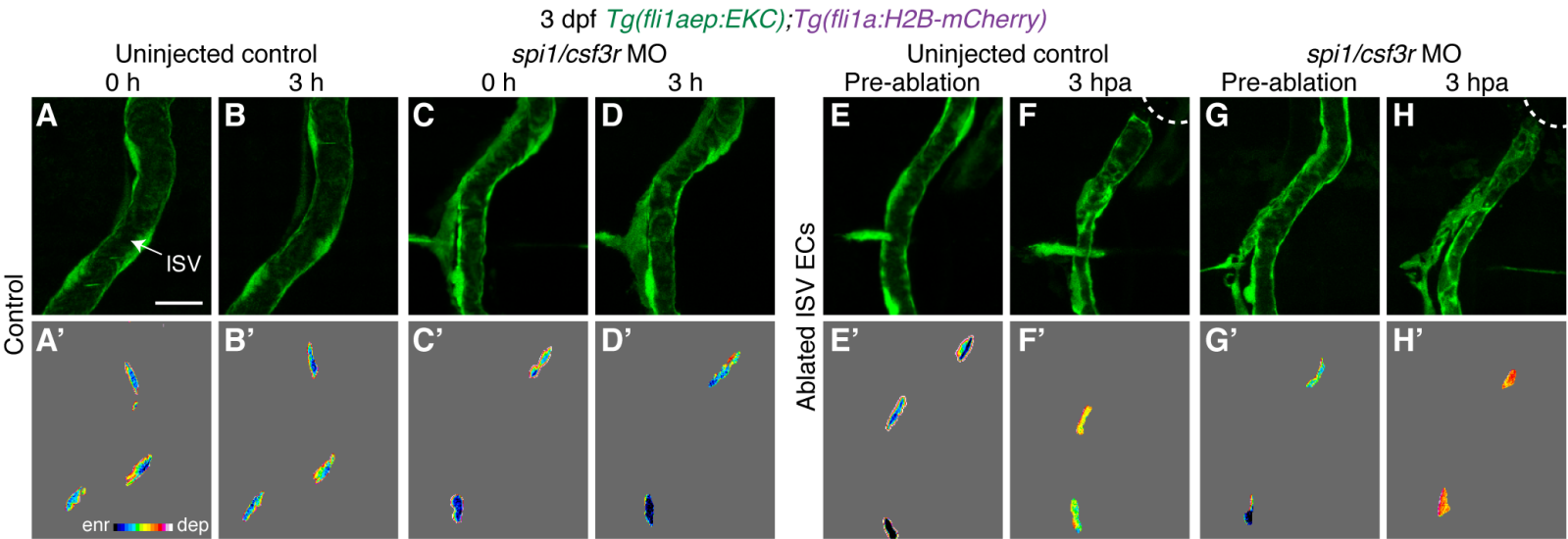






**Figure 6-figure supplement 1**

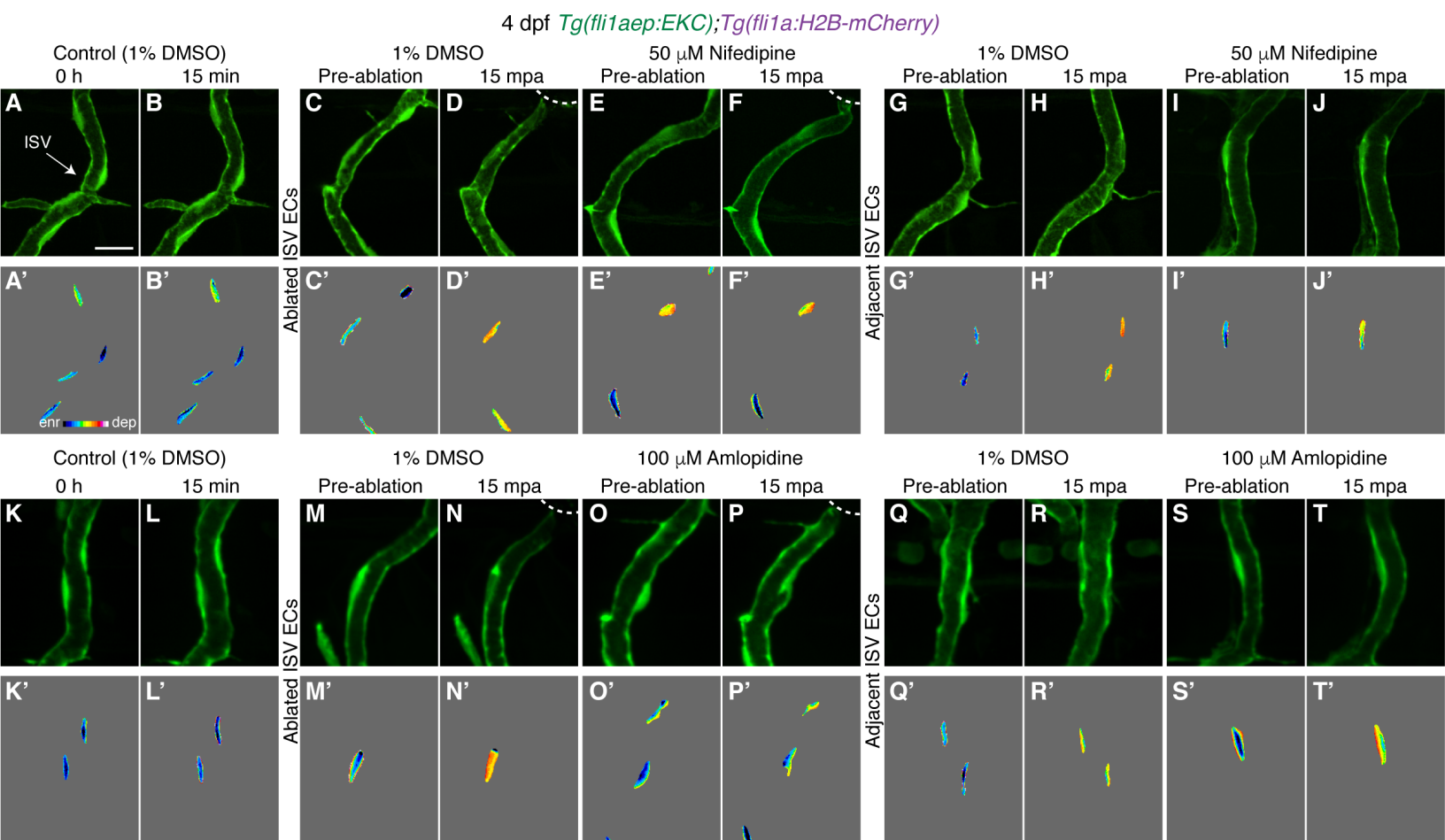


## Figure 6-figure supplement 2

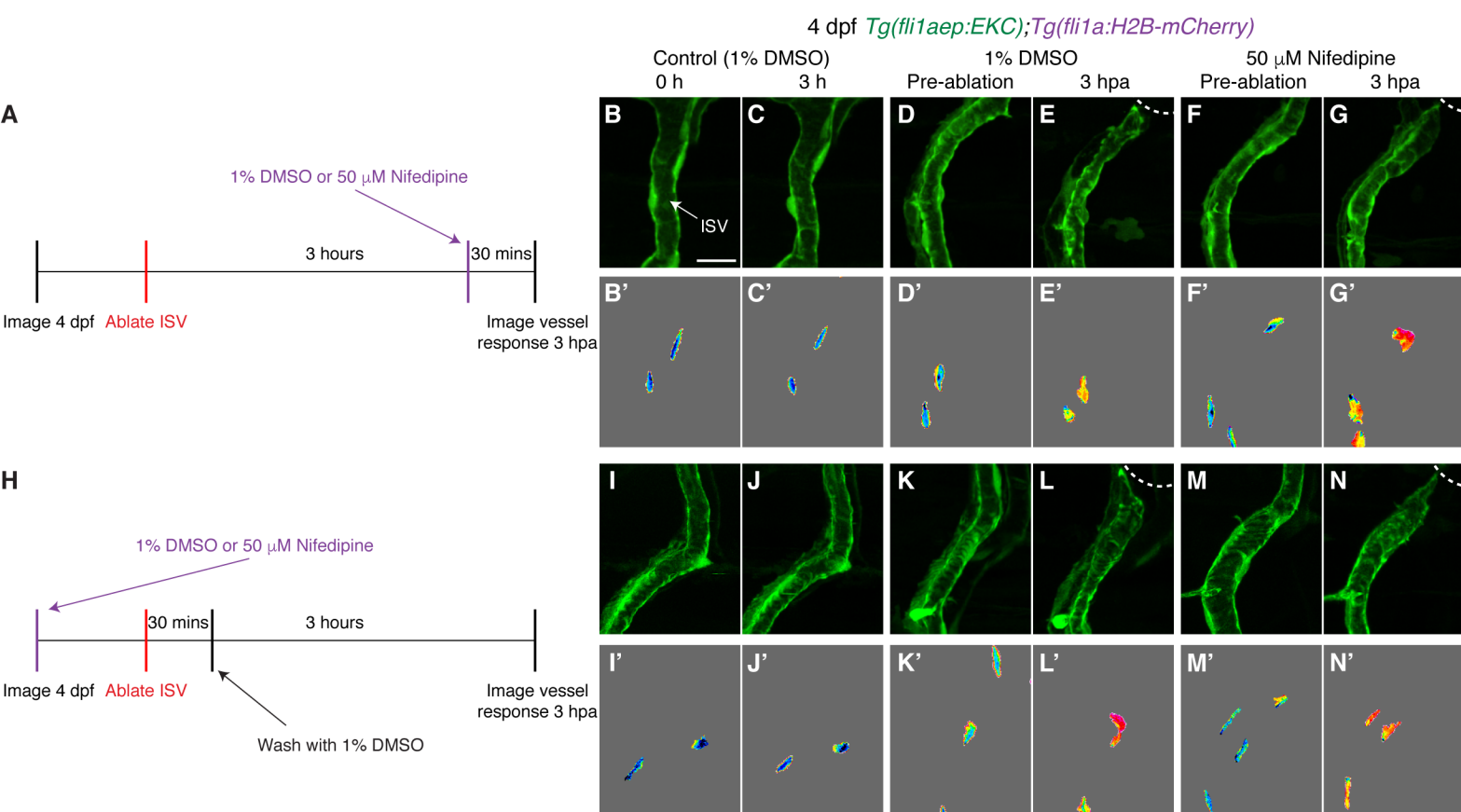




**Figure 7**

